Pergamon

PII: S0191-8141(96)00023-5

Journal of Structural Geology, Vol. 18, No. 7, pp. 951 to 970, 1996

0191-8141/96 $15.00+0.00

Generation and maintenance of abnormal fluid pressures beneath a ramping thrust sheet: isotropic permeability experiments

RICHARD E. SMITH* and DAVID V. WILTSCHKO

Department of Geology and Geophysics, Center for Tectonophysics, Texas A&M University, College Station, TX 77843-3113, U.S.A.

(*Received* 22 *December* 1995; *accepted in revised form* 11 *March* 1996)

Abstract—We have investigated the mechanisms responsible for the evolution of excess pore pressures within and beneath a ramping thrust sheet (i.e. fluid flow, porosity compression, and thermal expansion of water) and the sensitivity of pore pressure to a variety of physical parameters (e.g. permeability, thrust sheet velocity, heat flux). Coupled pore pressure and temperature equations were solved numerically in two dimensions using a generalized hydrostratigraphy of North American thrust belts. Because of the lack of either symmetry or a steady-state in this problem, both deposition and thrust loading stages were simulated. The dominant mechanisms controlling pore pressure evolution were fluid flow and compression of pore space by vertical loading; thermal expansion of the fluids was found to be insignificant in generating excess pore pressures at common thrust loading rates. The results indicate that it is possible to generate high pore pressure to lithostatic pressure ratios (λ) within thrust sheets by depositional loading prior to thrusting. High values of λ are generated and maintained during thrust loading for reasonable assumptions about the conditions thought to have existed in thrust belts. Values of λ were not constant throughout the model. The highest λ values tended to concentrate near the surface of the model and within and below the toe of the thrust sheet. The magnitude and distribution of excess pore pressures and λ values were found to be especially sensitive to variations in permeability. Excess pore pressure generation by compression exceeded pore pressure dissipation by fluid flow for permeabilities less than approximately 10^{-16} m^2; permeabilities greater than approximately 10^{-16} m^2 produced hydrostatic pore pressure gradients. The models demonstrate that permeability inhomogeneity due to lithologic variations may exert a strong control on the magnitude and spatial distribution of excess pore pressures within thrust sheets. In addition, these models indicate that it is unlikely that fluid pressure is high everywhere in a moving thrust sheet.

INTRODUCTION

Many models for the mechanics of fold and thrust belts hold that fluid pressure is locally, or even everywhere, abnormal, thus reducing the load necessary to move such large bodies of rock (e.g. Hubbert & Rubey 1959, Rubey & Hubbert 1959, Hsü 1969, Gretener 1972, Davis *et al.* 1983, Dahlen *et al.* 1984). These models have given us insight into how thrust sheets and accretionary prisms work and have been applied in a variety of compressional regimes worldwide. Yet despite the general acceptance of high fluid pressure as an important controlling mechanism for thrust motion, direct evidence for it in ancient continental thrust belts is either rare or ambiguous. Gretener (1977) describes as evidence for high fluid pressure 'basal tongues' of coaly shale, shale or gouge found at the bases of major thrust sheets in the Canadian Rocky Mountains and elsewhere. However, Brock & Engelder (1977) report that 'basal tongues' beneath the Muddy Mountain thrust show little evidence for the aid of abnormal fluid pressures in their injection. In fact, Axen (1984) argues against the role of fluid pressure for the nearby Keystone and Red Springs thrusts. Other reported evidence for the existence of high fluid pressure comes from the field data of Winslow (1983) who found that clastic dike swarms in the foreland region of the southern Andes were restricted to the frontal portions of major thrust sheets. These dikes were injected into thrust upper plates before significant formation of structural relief and therefore they may represent an example of material upwelling similar in mechanism found off the toe of some accretionary prisms (Westbrook & Smith 1983, Henry *et al.* 1990). Nevertheless, because the clastic dikes were injected before the development of significant fold structural relief, it is uncertain whether the fluid pressures existed during significant thrust motion. By contrast DiTullio & Byrne (1990) describe clastic dikes from the Shimanto belt accretionary prism, Japan, which were injected and deformed during the first phase of accretionary prism tectonism. As the restored attitudes of many of the dikes are subhorizontal (DiTullio & Byrne 1990, fig. 7), the fluid pressure in the clastic dikes was nearly lithostatic.

Recent work in active accretionary prisms has provided a wealth of information on the role of fluids in these environments. Chemosynthetic benthic communities, inorganic carbon deposits, *in situ* measurements of fluid discharge and a variety of fluid analyses suggest that fluid is moving through accretionary prisms (see Moore & Vrolijk 1992 for a recent review). Because fluid flows down a hydraulic head gradient, both ends of which may be characterized by nearly normal, i.e. hydrostatic, fluid pressure, this evidence alone is not necessarily proof of excess fluid pressure. However, there are a few rare unambiguous direct observations of fluid pressures in excess of hydrostatic (Chan 1964, Suppe & Wittke 1977, Moore *et al.* 1982). Moore *et al.* (1982) took advantage of the serendipitous sealing of a well through the frontal Barbados accretionary prism decollement to measure

*Present address: U.S. Army Corps of Engineers, 4735E Marginal Way S, Seattle, WA 98124-2255, U.S.A.

fluid pressure between 300 and 350 psi (21–24 bars) above normal. Moreover, the fault zone appeared to be highly permeable based on pumping tests. Chan (1964), Kuan (1967, 1968, 1971) and Suppe & Wittke (1977) document high pore fluid pressures in the frontal Taiwan accretionary prism from both direct measurements and sonic logs (see Davis *et al.* 1983). Overpressuring in this region begins at 1.5 to 4.1 km in depth, depending on locality, is controlled stratigraphically and corresponds to the change from what are interpreted to be interconnected permeable sands above to isolated sands embedded in, and underlain by, impermeable shales below. Suppe & Wittke (1977) made the observation that major thrust surfaces only occur within the overpressured section. Because there is little drill information from the more interior parts of the mountain belt, information does not exist on the role of excess fluid pressures in regions with significant faulting duration and displacement.

It is clear that there is a paucity of data on the role of abnormal fluid pressure in the mechanics of thrust sheets. For no thrust belt or accretionary prism do we have information on, (1) how the fluid pressure developed and, (2) how the fluid in a fault zone and elsewhere, dissipates with time. Given these uncertainties from observations, how can progress be made in understanding the existence and evolution of abnormal fluid pressures in fold and thrust belts? Why, for instance, after nearly 35 years of looking, are there so few well documented examples of abnormal fluid pressures in fold and thrust belts? Is the problem not having good diagnostic tools? Is there simply a lack of studies with the tools available? Given the fact that fluid flow is a potent means of reducing fluid pressure (e.g. Bear 1972, Palciauskas & Domenico 1989), are high fluid pressures transient? Does fluid pressure build and then dissipate quickly with the passage of, for example, a thrust toe? If so, are the volumes of fluid that are moved down pressure gradients (one end of which may be near lithostatic), so low as to leave little chance for their being recorded in vein fabrics or clastic dikes? Or, could the areas of abnormal fluid pressure be so small and in areas in which we normally have so little outcrop, such that the chance of their being observed is small. It is still clearly important to understand these questions. In fact, two objections originally raised to the Hubbert and Rubey hypothesis (e.g. Gretener 1981) must still be answered: (1) even if present before thrusting begins, how are excess fluid pressures maintained, especially since deformation leads to fracturing which may bleed the fluid pressure away from overpressured regions; (2) how does the high fluid pressure exist everywhere along a fault allowing simultaneous fault motion; or does it? Given that most wedge models assume that fluid pressure is abnormal and maintained that way throughout the history of the thrust belt, it is important to examine the evolution of fluid pressure in a typical thrust sheet.

Study goals

The purpose of this study is to develop a non-steady-state numerical model of pore pressure evolution in continental thrust belts to investigate the following: (1) whether or not high pore pressures could have been generated in ancient thrust belts given the conditions thought to have existed there, (2) the spatial distribution of the magnitude of pore pressures within a deforming thrust belt, (3) the maintenance of high pore pressures during thrusting, (4) the effects of lithological contrasts on pore pressure evolution, (5) the physical parameters that might be the most important in controlling the evolution of pore pressure in thrust belts, and (6) the conditions that may lead to over-pressuring prior to thrusting. This numerical model is based upon (1) the current understanding of the physical processes that control pore pressure development in a deforming, porous, elastic medium, (2) the known geometry and kinematic evolution of thrust belts, and (3) an investigation of the lithology-dependent physical properties (e.g. permeability and porosity) of thrust belts.

The working hypothesis of this study is that the evolution of excess pore pressure and paths of fluid flow within thrust belts are strongly dependent upon lithological contrasts among the sedimentary rocks comprising thrust belts. The philosophy of this study is not to model one particular spot in one thrust belt but rather to make the model applicable to thrust belts in general.

Previous work

The above questions have been addressed for accretionary prisms using coupled two-dimensional, thermo-poroelastic finite element models of non-steady-state pore pressure evolution (e.g. Shi & Wang 1988, Wang *et al.* 1990, Henry & Wang 1991). These models all show that high pore pressures may evolve in accretionary prisms and that fluid flow and compression of the rock matrix by loading are the dominant pore pressure dissipation and generation mechanisms, respectively. Since accretionary prisms share many geometrical and kinematic similarities with continental thrust belts (e.g. tectonic setting, convergence rate, and style of deformation), the evolution of high pore pressures within accretionary prisms suggests, by analogy, how high pore pressures may evolve in continental thrust belts.

With regards to continental thrust belts, Wang & Shi (1986) used a one-dimensional non-steady-state numerical model to determine how excess pore pressures may have evolved in the Taiwan fold and thrust belt. However, this study was designed to explore the specific case of Taiwan and no generalizations applicable to other thrust belts were made. The time dependent, two-dimensional temperature evolution within a ramping thrust sheet applicable to thrust belts in general was modeled by Shi & Wang (1987), but without thermal advection by fluid flow. Ge & Garven (1992) investigated the deformation and pore pressure evolution of the region in front of a thrust belt. In their numerical experiments the foreland is instantaneously loaded. They found that, (1) excess fluid pressure develops along the loaded edge, (2) flow rate in the order of cm/yr to m/yr are possible although less likely if the load rate is low and,

(3) stratigraphy plays a dominant role in determining if and where excess fluid pressures develop. In a model which includes a fault with independent hydraulic properties Ge & Garven (1994) found that these properties play a large role in determining the fluid pressure patterns in both the fault and footwall.

MODEL CONSTRUCTION

The new aspects of our model are, (1) fault-bend fold geometry, (2) changing geometry with thrust motion, (3) inhomogeneous permeability and (4) material properties appropriate for continental thrust belts. Like other models, fluid and solid mass balance are considered along with heat.

Pore pressure equation

We employed the following mass balance equation describing the change in total pore pressure with time for a fluid saturated, deforming medium as a function of fluid flow, mean stress, thermal expansion of water, and changes in porosity due to compaction (see Shi & Wang 1986 for a derivation):

$$\left[\frac{\alpha_n}{1-n}+n\beta\right]\frac{DP}{Dt}=\frac{1}{\eta}\nabla[k\nabla(P-\rho_w g d)]+\left[\frac{\alpha_n}{1-n}\right]\frac{D\sigma}{Dt}+[n\gamma_w]\frac{DT}{Dt}+\frac{1}{1-n}\left[-\frac{\partial n}{\partial t}\right] \quad (1)$$

where α_n is the porosity compressibility, n is the porosity, β is the compressibility of water, P is the total pore pressure, η is the viscosity of water, k is the permeability, ρ_w is the density of water, g is the acceleration due to gravity, d is the depth below the surface of the model, σ is the mean stress, γ_w is the thermal expansion coefficient of water, and T is the temperature. D/Dt denotes a material time derivative. The first term on the right hand side of equation (1) is the diffusion term which describes the dissipation of excess pore pressures through fluid flow. The other three terms on the right hand side of equation (1) are source terms of excess pore pressure. The second term on the right represents mechanical pressuring due to tectonic compression or increases in overburden due either to sedimentation or thrust loading; in our study we only consider increases in overburden due to either sedimentation or thrust sheet emplacement. The third term represents aquathermal pressuring from the expansion of the pore fluid with increasing temperature. The fourth term represents the change in the porosity with time due to creep of the solid skeleton of the matrix under stress. Neither fracture formation, which is potentially an important dissipative mechanism of pore fluid pressure, nor temperature induced phase transformations of shaly rocks which may increase fluid pressure by releasing fluids, were treated in our study.

Equation (1) is based upon several assumptions. The compressibility of the solid grains was assumed zero because the compressibility of the solid grains is very small relative to the compressibility of the pore space. Porosity change is considered reversible and conservative. That is, the bulk response of the porous material is elastic. The thermal expansion coefficients of the solids and the bulk porous body were also assumed zero because they are very small compared to the thermal expansion of water. The effective stress is assumed equal to the mean stress minus the pore pressure, which is reasonable for sedimentary rocks (Paterson 1978). Finally, pore pressure changes due to shear stress are ignored. By ignoring shear stresses, a potential source of pore pressure generation is neglected. Thus, this equation underestimates the magnitude of pore pressure due to loading.

Heat equation

We used the following constitutive equation for heat transfer by advection and convection:

$$c\rho_b\frac{DT}{Dt}=-c_w\rho_w\vec{q}\nabla T+K_T\nabla^2T+Q \quad (2)$$

where c is the bulk specific heat, ρ_b is the bulk density of the water saturated rocks, c_w is the specific heat of water, $\vec{q}$ is Darcy's flux, K_T is the bulk thermal conductivity of the rocks and fluid, and Q is a heat source term. The first term on the right hand side of equation (2) is the advective heat flow due to the flow of the fluid. Advective heat transfer due to the motion of the solid matrix is handled implicitly by the material derivative term on the left hand side of equation (2). The second term on the right represents conductive heat transfer through the solids and the fluid; and the third term represents heat sources (e.g. radioactive elements).

Equation (2) is based upon several assumptions. The bulk specific heat and the specific heat of water are assumed constant. These two parameters are likely to vary somewhat as porosity changes due to compression of the pore space by loading. The bulk thermal conductivity of the rocks and fluid is assumed homogeneous and constant. However, the thermal conductivity of rocks can vary according to rock lithology, and the bulk thermal conductivity of the rock and fluid will vary with porosity changes due to loading. The fluid and the solid are assumed to always be in thermal equilibrium, which is likely to be valid only if fluid motion is slow relative to the rate of heat transfer into the solid matrix. The energy associated with the deformation of the rock matrix and pore fluid is assumed zero, thus eliminating a potential heat source. Finally, shear stresses in the fluid are ignored.

Upper limit of pore pressure

The effects of fracture and vein formation on the pore pressure were ignored. However, fracture formation is potentially a very important mechanism of dissipating high pore pressures because fractures can increase the permeability of relatively impermeable rocks by up to 1000 times (Davis 1969) and simultaneously increase the

pore space by dilation. In our study, no upper limit was set on the value of pore pressure, and hence pore pressure was allowed to exceed the mean stress despite the likelihood that fracturing would limit the ultimate value of pore pressure. Therefore, modeled zones with pore pressure values in excess of the mean stress should be interpreted as concentrations of relatively high pore pressures where rock failure is likely.

North American thrust belt stratigraphy

We employed a schematic hydrostratigraphy (Domenico & Schwartz 1990) for North American thrust belts in our model. In Fig. 1(a) a typical stratigraphic column is illustrated. The schematic hydrostatigraphy derived from a compilation of other typical stratigraphic columns from North America (Smith 1992) is shown in Fig. 1(b). The four common elements of stratigraphy that are incorporated into Fig. 1b are: (1) a lower, mostly shaley layer, (2) a middle carbonate layer, (3) an upper layer of mixed sandstones, siltstones and shales that are probably related to deposition within a foreland basin, and (4) a crystalline, igneous or metamorphic basement largely uninvolved in thrust faulting.

Material properties of the rocks and fluid

Permeability. Permeability is a function of lithological characteristics and stress state. Grain size and sorting are the primary lithological characteristics that control permeability. Rocks with a large grain size tend to have higher permeabilities than rocks with a smaller grain size. Similarly, well sorted rocks tend to have higher permeabilities than poorly sorted rocks due to the reduction of pore space by fine grained particles occupying the space between larger grains. Chemical and diagenetic processes that affect permeability by changing the lithology are dissolution, recrystallization, cementation, and mineral transformations. Mechanical deformation can influence permeability by both the formation of fractures and the reduction of porosity due to compaction caused by increased overburden.

We have compiled Fig. 2 in order to constrain the range of permeabilities representative of continental, particularly North American, thrust belt rocks. Sandstones tend to have higher permeabilities than siltstones which in turn have higher permeabilities than shales. The carbonates, which include both limestones and dolomites, span a large range of permeabilities with very fine grained carbonates having the lowest permeabilities (Brace 1980) and coarse grained or karstic carbonates having the highest permeabilities. In general, the greater number of measurements of carbonate rocks used to compile Fig. 2 had permeabilities greater than 10^{-17} m^2. Therefore, it can be concluded that in general, carbonates and sandstones tend to be highly permeable relative to siltstones and shales.

The values of permeability in Fig. 2 were collected from laboratory specimens. It has been argued (Davis 1969, Brace 1980, Clauser 1992) that permeability is a

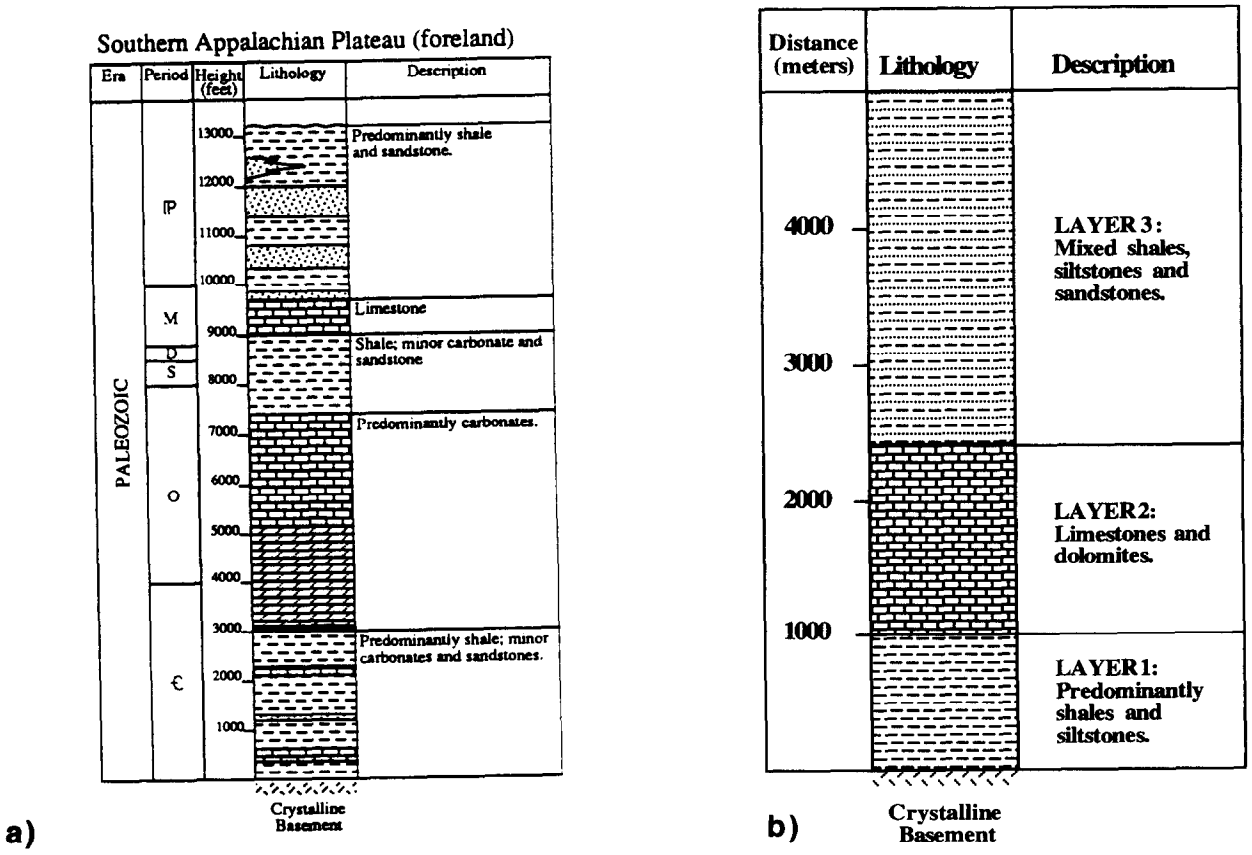

Fig. 1. Hydrostratigraphy used in the model. (a) Generalized stratigraphic column of the sedimentary rocks involved in thrust deformation of the Pine Mountain thrust sheet, Southern Appalachian Plateau, Kentucky–Tennessee. Column compiled from data by Englund (1964), Englund *et al.* (1964), and Harris & Milici (1977). (b) Generic stratigraphy of North American thrust belts.

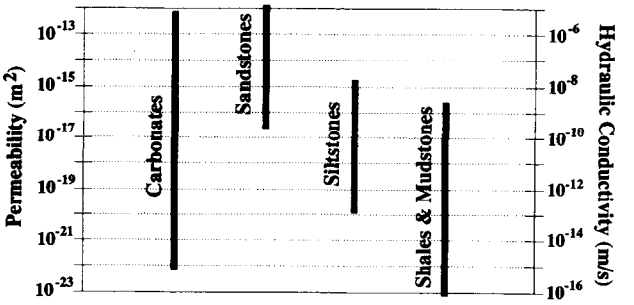

Fig. 2. Permeability and equivalent hydraulic conductivity ($\eta = 0.001$ Pa·s, $\rho_w = 1000$ kg/m^3) of common sedimentary rocks measured on laboratory specimens. Data compiled from Davis (1969), Brace (1980) and Domenico & Schwartz (1990).

function of the scale at which it is measured. Laboratory measurements are typically made in samples devoid of discontinuities such as faults and bedding planes, and therefore produce values of an order of magnitude smaller than by other means such as *in situ* measurements which include discontinuities. However, *in situ* measurements of permeability (Brace 1980), which record fracture permeability, still fall within the broad range of permeabilities for sedimentary rock types as measured in laboratory samples.

Laboratory measurements of permeability are available for some of the lithologic units of the Idaho–Wyoming–Utah thrust belt. Merewether *et al.* (1984) reported permeabilities of 1.4×10^{-16} m^2 to 6.8×10^{-15} m^2 for sandstones of the Frontier Formation of Wyoming, which is modeled as part of Layer 3 (Fig. 1b). Thayer (1983) reported horizontal permeabilities ranging from less than 1×10^{-17} m^2 to 3.9×10^{-13} m^2, and vertical permeabilities from less than 1×10^{-17} m^2 to 9×10^{-13} m^2 with a mean permeability of 1.58×10^{-14} m^2 for the Madison Limestone, which is also present in the Idaho–Wyoming–Utah thrust belt, and is modeled as part of Layer 2 (Fig. 1b). Both studies report permeability values that fall within the ranges illustrated in Fig. 2 for their respective lithologies. In this study we have ignored chemical and diagenetic effects on permeability.

For the mechanical effects, experimental results on sandstones (Wilhelm & Somerton 1967, Mordecai & Morris 1971, Daw *et al.* 1974, Zoback & Byerlee 1976) indicate that with increasing differential stress, permeability tends to decrease generally by less than 50% due to compaction of the matrix. At approximately two-thirds of the ultimate strength of the rock, permeability begins to increase as fractures develop (Zoback & Byerlee 1976). The change in permeability due to compaction is insignificant when compared to the potential range of permeability values for sedimentary rocks (Fig. 2). Further, permeability is potentially much more sensitive to fracture development than compaction (Daw *et al.* 1974, Jones 1975) because fracture permeability can be up to 1000 times greater than unfractured permeability. Despite this fact, permeability was modeled as constant with respect to time because (1) permeability changes due to compaction alone are small relative to the range of possible permeabilities of sedimentary rocks, and (2) data for the more important mechanical mechanisms affecting permeability and fracture development, are not available. We chose instead to explore the influence of a wide range of constant (though inhomogeneous) permeabilities.

Since thrust sheets are composed of a variety of sedimentary rock types including both potentially low permeability shales and potentially high permeability carbonates and sandstones, thrust belts are likely to have vertically inhomogeneous permeability. It is also likely that thrust belts are horizontally inhomogeneous with respect to permeability due to stratigraphic pinch outs and/or facies changes. Horizontal changes are difficult to generalize and therefore were not considered for this study.

For the numerical models in this study, it was necessary to assign representative values of permeability to the rocks comprising the model. For the model generic North American stratigraphy (Fig. 1b), the lowermost layer of shales and siltstones (Layer 1) should tend to have low permeabilities ranging from 10^{-16} m^2 to 10^{-20} m^2 (Fig. 3). The middle carbonate layer (Layer 2) may have a relatively high permeability ranging from 10^{-12} m^2 to 10^{-16} m^2. The uppermost mixed clastics unit (Layer 3) should then have permeability values between that of low permeability shales and high permeability sandstones.

Porosity. Porosity, like permeability, is a function of lithologic characteristics, chemical and diagenetic effects, and mechanical deformation. A constitutive equation for porosity is required for the last term of equation (1). Porosity was therefore modeled empirically as a function of effective stress (Shi & Wang 1986):

$$n = n_0 \exp(-bP_e) \tag{3}$$

where n_0 is the surface porosity, b is an empirically derived material parameter, and P_e is the effective stress (mean stress minus the pore pressure). Figure 3 illustrates porosity as a function of depth curves compiled for various sedimentary rocks in 'non-tectonic' basins such as the Gulf Coast. Clearly, there is a large variation in the porosity as a function of depth for common sedimentary rocks. Shi & Wang (1986) determined that shales have values of b in the order of 10^{-8} to 10^{-7} Pa^{-1}, and that sandstones have values of b in the order of 5×10^{-9} to 5×10^{-8} Pa^{-1}. However, the data trends presented in Fig. 3 do not appear to correlate with lithology. Instead, some factor other than lithologic characteristics (e.g. age of rocks or degree of lithification) may control the value of b. Due to this lack of clear lithologic control of the value b, it was assumed that all rocks modeled in this study would be homogeneous with regards to porosity as a function of effective stress. It was further assumed that the rocks comprising thrust belts tend to be older, previously lithified rocks that would, therefore, have a low rate of porosity reduction with increasing effective stress as compared to younger unconsolidated sediments. By assuming that effective stress was equal to the lithostatic stress minus the hydrostatic pore pressure, porosity as a function of depth for a b value of 1×10^{-8} Pa^{-1} was also plotted on Fig. 3. The value of 1×10^{-8}

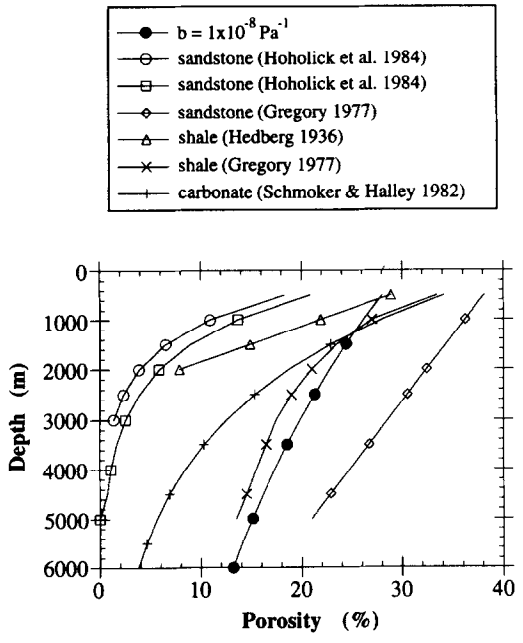

Fig. 3. Porosity compaction as a function of depth for six rocks in non-tectonically disturbed basins, and porosity as a function of depth, assuming hydrostatic pore pressure and using the relation, $n = n_0 \cdot \exp(-bP_e)$. Data taken from Hedberg (1936), Gregory (1977), Schmoker & Halley (1982) and Hoholick *et al.* (1984).

Pa^{-1} was used as the standard value of b for all models on the assumption that older, consolidated sedimentary rocks representative of thrust belts would tend to be more rigid than younger, relatively unconsolidated rocks and, therefore, would compact less easily.

Compressibility. Typical values of porosity compressibility (α_n) for sedimentary rocks range from 1×10^{-8} Pa to 1×10^{-11} Pa (Birch 1966, Palciauskas & Domenico 1989) where shaly rocks tend to be somewhat more compressible than sandstones and carbonates. A mid-range value of 1×10^{-10} Pa^{-1} for α_n was chosen as representative of older, indurated sedimentary rocks. However, because deformation within a thrust belt occurs over periods of tens of millions of years, inelastic deformation undoubtedly takes place. Palciauskas & Domenico (1989) theoretically treat the irreversible process of pressure solution in a sandstone and determine that the inelastic value of α_n is 50 times greater than for elastic deformation for a time scale on the order of millions of years. It was assumed for this study that this conclusion is applicable to all rock types. Therefore, a value of 5×10^{-9} Pa^{-1} was used as the homogeneous standard for all models.

The compressibility of water is a function of pressure and temperature (Strauss & Schubert 1977), but the value of compressibility does not vary much for the conditions present in this model so a constant value of 5×10^{-10} Pa^{-1} was assumed.

Thermal properties. The thermal expansion of water is a function of pressure and temperature, but the variation is small for the conditions typical of the models in this study (Shi & Wang 1986). Therefore, a constant value 5×10^{-4}°C^{-1} was used. The thermal conductivities of sedimentary rocks range from 1 to 5 W/m°C (Clark 1966, Turcotte & Schubert 1982). Because this range is small and the various lithologies tend to share similar values, a constant value of 3 W/m°C was used for all rock types in this model. The thermal conductivity of water is a function of pressure and temperature (Clark 1966), but the variation is not great over the range of conditions that prevail in this model so a constant value of 0.7 W/m°C was used for all models. The bulk thermal conductivity of the saturated rock matrix was calculated from the following relation (Lewis & Rose 1970):

$$K_T = K_r \frac{K_w}{K_r}^n \quad (4)$$

where K_r is the thermal conductivity of the rock and K_w is the thermal conductivity of the water. The bulk thermal conductivity was also treated as a constant using an average porosity value of 0.15.

The specific heat of water exhibits only a slight temperature dependency for the range of conditions in this study (Lide 1991), so a constant value of 4.2×10^3 J/kg°C was used in all models. Data on the specific heat of rocks is sparse, but available data (Touloukian *et al.* 1981, Lide 1991) suggest that 850 J/kg°C is an appropriate average value for most sedimentary rocks. The bulk specific heat was calculated using a volume fraction weighting scheme (Shi & Wang 1986)

$$c = c_w n + c_r(1 - n) \quad (5)$$

where c_r is the specific heat of the rock. The bulk specific heat was also treated as a constant using an average porosity value of 0.15.

Geometry and kinematics

A model of pore pressure evolution in thrust belts requires knowledge of the geometry and kinematics of thrust belts. We have used a stair-step shape for the model thrust fault, as first described by Rich (1934) for the Pine Mountain thrust fault. Rates of thrust slip have been deduced for thrust sheets within the Wyoming thrust belt of about 0.5 cm/yr (Wiltschko & Dorr 1983), about 0.16 to 0.22 cm/yr for those within the Canadian Rockies (Elliott 1976) and up to 1.5 cm/yr for the Precordillera between 30 and 31°S, Andes (Jordan *et al.* 1993). We employed a value of 0.5 cm/yr for these experiments.

The kinematic evolution of the two-dimensional model consists of two phases (Fig. 4). In the first phase, the three sedimentary layers of the model stratigraphy are deposited each at a constant rate with no interruption of deposition between layers. Deposition rates for the rocks summarized in Fig. 1(b) were taken from Perrodon & Masse (1984). A thrust ramp with an inclination of approximately 27° is then artificially imposed within the deposited sedimentary rocks at the beginning of the second thrust loading phase. Model thrust motion was constant and the vertical back boundary of the model,

representing the hinterlandward boundary of the thrust sheet, moved with the hanging wall along the décollement. The geometry of the deforming hanging wall was modeled using fault-bend folding (Suppe 1983) which conserves the area of the folded sedimentary layers. To model the general wedge shape typical of thrust belts, simulate deposition from the hinterland, and to maximize fluid pressure, material was deposited in the region between the vertical back boundary and the ramp anticline at a rate equal to the vertical velocity component of the moving hanging wall. This model basin is analogous to an intermontane basin. This syntectonic depositional material was assigned physical properties identical to Layer 3 (top most). It was assumed that no erosion occurred during thrusting. Thrust motion was stopped once the stratigraphic section was doubled.

The mean stress was assumed always to be equal to the weight of the overburden ($\rho_b g d$). Therefore, spatial and temporal changes in stress resulted only from changes in the lithostatic component of stress due to sediment deposition and/or thrust loading.

Numerical formulation

Equations (1) and (2) were used to model the evolution of pore pressure and temperature, respectively, for the two-dimensional model. Because these equations cannot be solved analytically, a fully explicit finite difference technique was used to approximate the solution.

A fixed, rectilinear grid of nodes was set up through which the material of the upper thrust sheet moved. The spacing between nodes varied, depending on the model run, between 250 and 500 m in the z-direction and between 500 and 1000 m in the x-direction. In all cases the horizontal node spacing was twice the vertical node spacing. The spacing was changed depending on the length of computation time required for a particular numerical experiment. Tests were run to determine the effect of node spacing on the solution and it was found that the solutions were relatively insensitive to the differences in node spacings used.

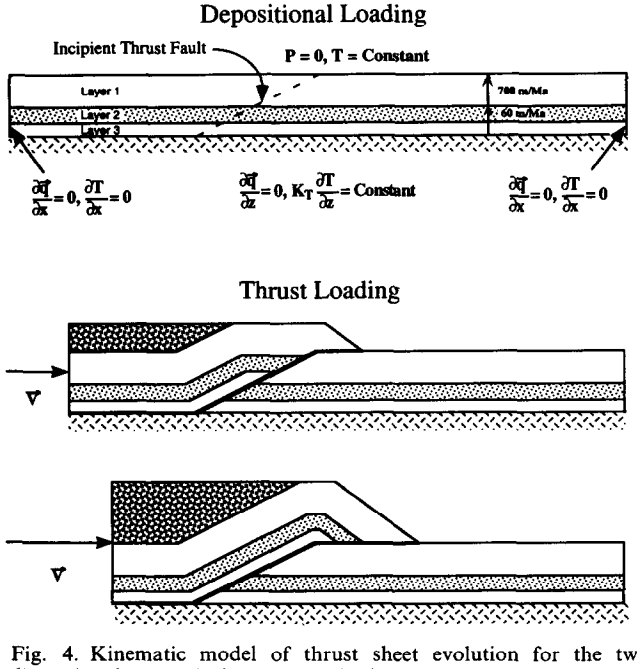

Fig. 4. Kinematic model of thrust sheet evolution for the two-dimensional numerical model. Stippled region behind fault-bend anticline represents syntectonic deposition from the hinterland.

To simulate the coupling of the pore pressure equation (1) and the heat equation (2), the temperature for all nodes was calculated for the current time step using the values of pressure and temperature from a previous time step. The pore pressure for all nodes was then calculated for the current time step using the values of pressure from the previous time step and the temperature values just calculated for the current time step. The only material parameter allowed to change with time was porosity. Porosity values for each node were updated each time step prior to the temperature calculations based upon the value of the effective stress from the previous time step. The maximum value of the time step for a fully explicit finite difference solution is limited by the stability criterion (Smith 1985) of the pore pressure and temperature solutions. The smaller of the two times steps computed for the pore pressure and temperature calculations was used. Tests showed that reducing the time step below this value had little or no effect on the numerical results. To reduce the computation time of the model, the deposition loading portion of the two-dimensional model was solved in one vertical dimension. This one-dimensional simplification is justified because the assumed hinterland and foreland boundary conditions prevent horizontal fluid flow and the uniform vertical loading across the model is unlikely to produce horizontal excess pore pressure gradients to drive horizontal fluid flow. A similar argument can be made against spatial variations in temperature and porosity. Therefore, the values of pore pressure during deposition are likely to be constant horizontally.

The first bracketed term on the right hand side of (1) is the fluid flux, $\vec{q}$, defined as

$$\vec{q} = -\frac{k\rho_w g}{\eta}\nabla h \tag{6}$$

where h is the head defined as

$$h = z + P/\rho_w g \tag{7}$$

where z is height above some datum. The first and second terms of the head are the elevation and pressure heads, respectively. The velocity head is ignored. Converting z to a measure involving depth from the surface,

$$z = H - d \tag{8}$$

where H is the total thickness of the thrust sheet and d is depth at a particular x. Then $h = H - d + P/\rho_w g$ so that

$$\vec{q} = -\frac{k}{\eta}\nabla(P - \rho_w g d) \tag{9}$$

which is used in deriving (1).

Boundary conditions

The upper and lower fluid flow boundary conditions are zero pore pressure and no flow, respectively (Fig. 4a). The vertical foreland boundary is also assumed to be a no flow boundary and is placed far in front of the toe of the thrust sheet to minimize the boundary's effect upon fluid flow near the toe of the moving thrust sheet. The hinterland vertical boundary was assumed to be an impermeable boundary.

The thermal boundary conditions included a constant temperature surface boundary, two vertical zero flux boundaries, and a lower constant flux boundary. The surface temperature was assumed to be 7°C for all numerical experiments. An average thermal flux for continental terrains of 57 mW/m^2 (Turcotte & Schubert 1982) was used as the standard thermal flux at the base of the models in this study. Values of 40 and 80 mW/m^2 representing the extremes measured for orogenic terrains (Bott 1971) were also modeled.

RESULTS

The numerical solutions of the governing equations that control the evolution of pore pressure and temperature in a thrust belt are dependent upon a number of material parameters, some of whose values can vary over a large range (e.g. permeability). Therefore, a series of numerical experiments was run to (1) test the sensitivity of the numerical solution to various parameters, and (2) determine what conditions are favorable or unfavorable for the development of excess pore pressures in a thrust belt. We report here on the following analyses which are intended to determine the effects on the pore pressure of: (1) variations in permeability for a homogeneous thrust sheet and its footwall, (2) variations of porosity compressibility, and (3) the effect of permeability inhomogeneity using the generic North American thrust belt stratigraphy. For all of the numerical experiments run for this study, a set of values of all of the material parameters needed for the numerical solution of equations (1) and (2) was chosen as a representative standard (Table 1) by which variations in the values of individual parameters could be compared. Unless otherwise stated, standard values of all parameters were used.

Values of the total pore pressure, temperature, and porosity were calculated for all nodes and for all time steps during the evolution of the two-dimensional model. Values of the excess pore pressure, defined as

$$P' = P - \rho_w g d \tag{10}$$

and the Hubbert and Rubey parameter λ (hydrostatic to pressure ratio)

$$\lambda = \frac{P}{\rho_b g d} \tag{11}$$

were determined separately after each numerical experiment was run to save computer time.

To allow easy comparison of the effects of variations in material parameters, the entire evolutionary sequence of all of the calculated parameters will not be presented for each numerical experiment. Instead, the final time step will be illustrated for each numerical experiment along with the final time step of other numerical experiments with different values of the material parameter being tested. To illustrate the evolution of the calculated parameters during thrust motion, the evolutionary sequences during thrust loading of total pore pressure (Fig. 5), excess pore pressure (Fig. 6), λ (Fig. 7) and temperature (Fig. 8) are presented for a numerical experiment that used only the standard material parameter values (Table 1). The permeability was considered homogeneous and isotropic for this numerical experiment. The lines designating the lithologic boundaries of the generic North American stratigraphy are plotted on all figures for reference when comparing results of inhomogeneous stratigraphic sequences discussed later. For the standard thrust velocity of 0.5 cm/yr, the continuous sequence of modeled thrust motion took approximately 2.2 Ma. Deposition loading required a modeled time of approximately 44 Ma for the thicknesses and rates of deposition considered.

Prior to thrusting, the pore pressure increased uniformly from top to bottom of the model rocks (Fig. 5a). With thrust displacement, the orientation of the pore pressure gradient became disturbed beneath the toe of the thrust sheet, and within the thrust sheet near the base of the thrust ramp (Fig. 5b). This disturbance of the gradient orientation remained throughout thrust deformation (Fig. 5c & d). The lines of equal pore pressure tended to parallel the topography of the model everywhere except immediately above and below the thrust sheet, with pore pressure contours dipping downward and bulging upward above and below the ramp, respectively. Pore pressures immediately above the thrust ramp are slightly depressed relative to nearby values due to the lack of vertical loading for material points within the thrust ramp. This effect seems to be concentrated near the first kink plane of the fault-bend fold which is a singularity where deposition loading behind the thrust anticline ends abruptly. The upward bulge of pore

Table 1. Standard values and ranges tested of the material parameters used to solve the two-dimensional models

Parameter	Standard model values	Range tested
k	10^{-18} m^2	10^{-14} to 10^{-20} m^2
n_0	0.3	
b	1×10^{-8} Pa^{-1}	
α_n	5×10^{-9} Pa^{-1}	0 to 1×10^{-8} Pa^{-1}
β	5×10^{-10} Pa^{-1}	
ρ_b	2400 kg/m^3	
ρ_w	1000 kg/m^3	
γ_w	7.5×10^{-4}°C^{-1}	
η	0.001 Pa·s	
c_r	850 J/kg°C	
c_w	4200 J/kg°C	
K_r	3 W/m°C	
K_w	0.7 W/m°C	
$K_T \delta T/\delta z$	0.057 W/m^2	
v_{thrust}	0.5 cm/yr	

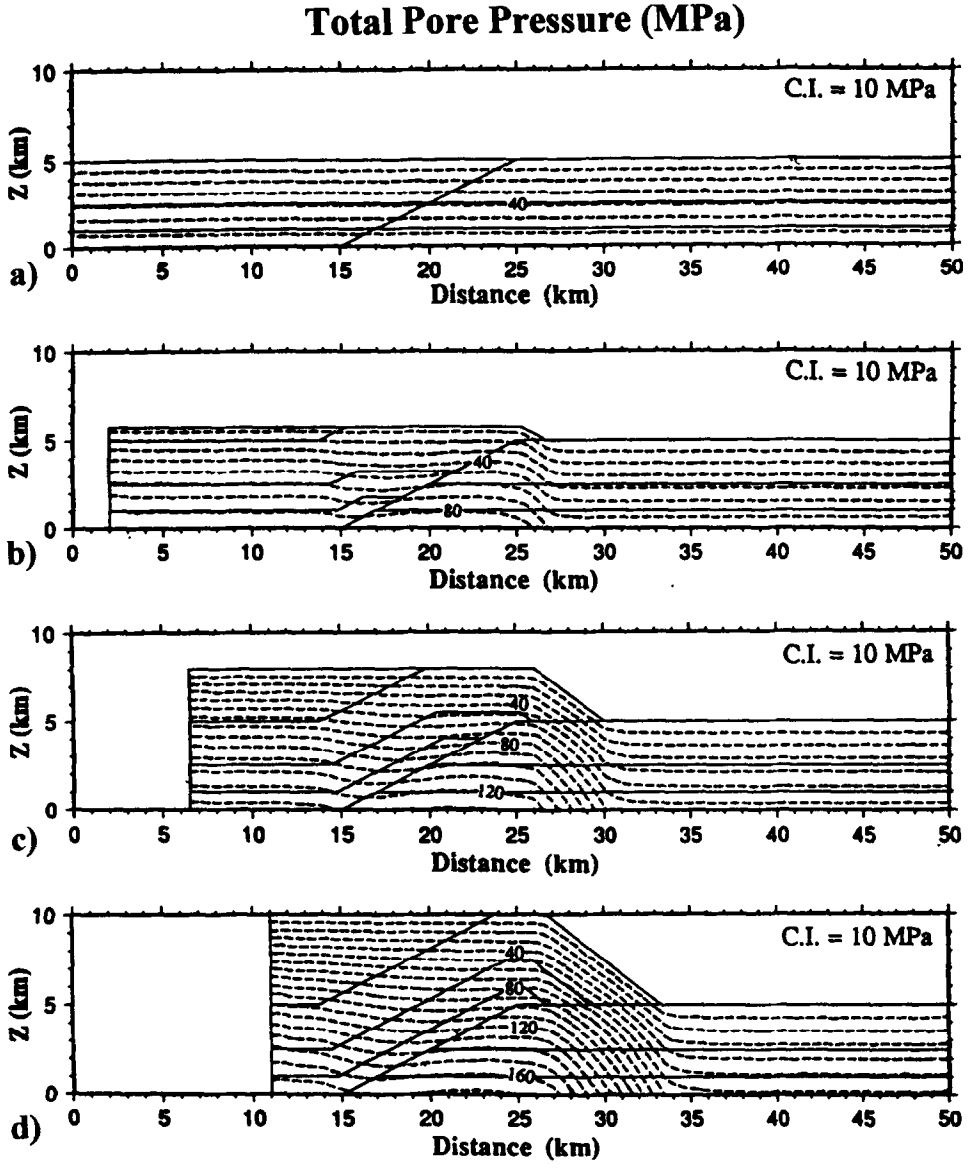

Fig. 5. Evolution of total pore pressure within a thrust sheet with homogeneous and isotropic permeability of 10^{-18} m^2 and all other material parameters at standard values (Table 1). (a) Prior to thrusting, after deposition. (b) After 2 km of motion (18% of total). (c) After 6.5 km (60%). (d) At the end of thrusting where the section at the top of the ramp is doubled. C.I., contour interval in this and all subsequent figures.

pressure beneath the thrust ramp is due to loading of those modeled rocks beneath the thrust sheet by the moving thrust sheet.

The orientations of the excess pore pressure contours (Fig. 6) are similar to the total pore pressure contours. The highest excess pore pressure values are in the extreme hinterland and beneath the thrust ramp because these two areas were loaded by increasing vertical stress due to deposition loading and thrust loading, respectively, during the model's evolution. Excess pore pressure values are depressed within the unloaded region of the thrust sheet above the thrust ramp. Excess pore pressure values would obviously be much lower in the hanging wall in the absence of syntectonic deposition.

Fluid flow is driven by excess pore pressure gradients, and the direction of fluid flow is normal to the equipotential excess pore pressure contours. Therefore, fluid flow is generally upward within the hanging wall (Fig. 6b–d) during thrusting. The area immediately above the thrust ramp receives flow from both the hinterland and footwall. Beneath the thrust toe, excess pore pressure contours are nearly vertical so that fluid flow is horizontal, indicating that fluid in this region is flowing into the foreland.

Values of λ are high at the end of deposition (Fig. 7a) indicating conditions favorable for thrust motion were present prior to thrusting. During thrusting, the highest values of λ are concentrated within and immediately beneath the toe of the thrust sheet as well as in the hinterland portion of the thrust belt (Fig. 7b–d). The value of λ decreases steadily in the foreland region as pore pressure decays in the absence of loading. During all stages of loading, the highest values of λ are nearest the surface of the model.

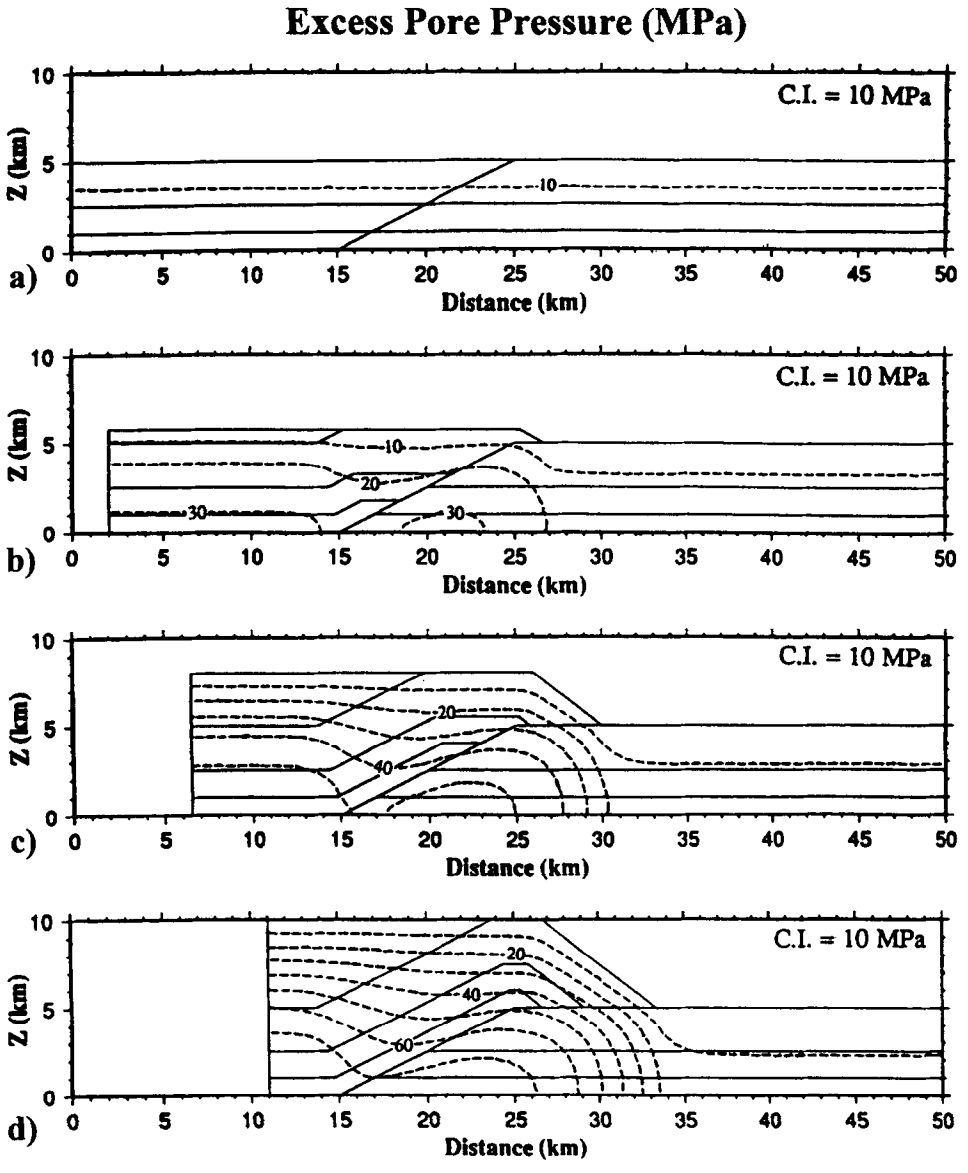

Fig. 6. Evolution of excess pore pressure within a thrust sheet with homogeneous and isotropic permeability of 10^{-18} m^2 and all other material parameters at standard values (Table 1). (a) Prior to thrusting, after deposition. (b) After 2 km of motion (18% of total). (c) After 6.5 km (60%). (d) At the end of thrusting where the section at the top of the ramp is doubled.

A normal geothermal gradient of about 25°C/km was generated during model deposition loading (Fig. 8a). During thrusting, this gradient was disturbed within and beneath the thrust sheet and was reduced to about 20°C/km (Fig. 8b–d). However, the thermal contours still formed a subdued replica of the topography. In subsequent tests it was found that pore pressure results are insensitive to changes in both thermal flux at the base of the model and surface porosity, b (equation 3).

Permeability numerical experiments

A range of permeabilities of 10^{-16} to 10^{-20} m^2 for a thrust belt with homogeneous stratigraphy was tested to determine the sensitivity of pore pressure to permeability and to determine what values of permeability are likely to cause over-pressuring. As expected, the lowest permeability value, 10^{-20} m^2, produced the highest values of excess pore pressure (Fig. 9a), with excess pore pressures approaching lithostatic, $\lambda = 1$ (Fig. 10a) throughout the model. Excess pore pressure and corresponding λ values decreased steadily with increasing permeability (Figs. 9b–d and 10b–d). A homogeneous permeability of 10^{-16} m^2 produced no excess pore pressures whatsoever. The thermal solution was identical for the range of permeabilities tested suggesting that either, (1) thermal conduction dominated over thermal transfer by fluid advection for the tested range of permeabilities or, (2) even very slow fluid flow causes rapid heat transfer and thermal equilibrium.

Pore pressure is clearly sensitive to order-of-magnitude changes in the permeability. Rocks with permeabilities of the order of 10^{-16} m^2 or greater will dissipate pore pressures faster then they can be generated for the standard conditions modeled, while rocks with lower permeabilities will generate excess pore pressures faster

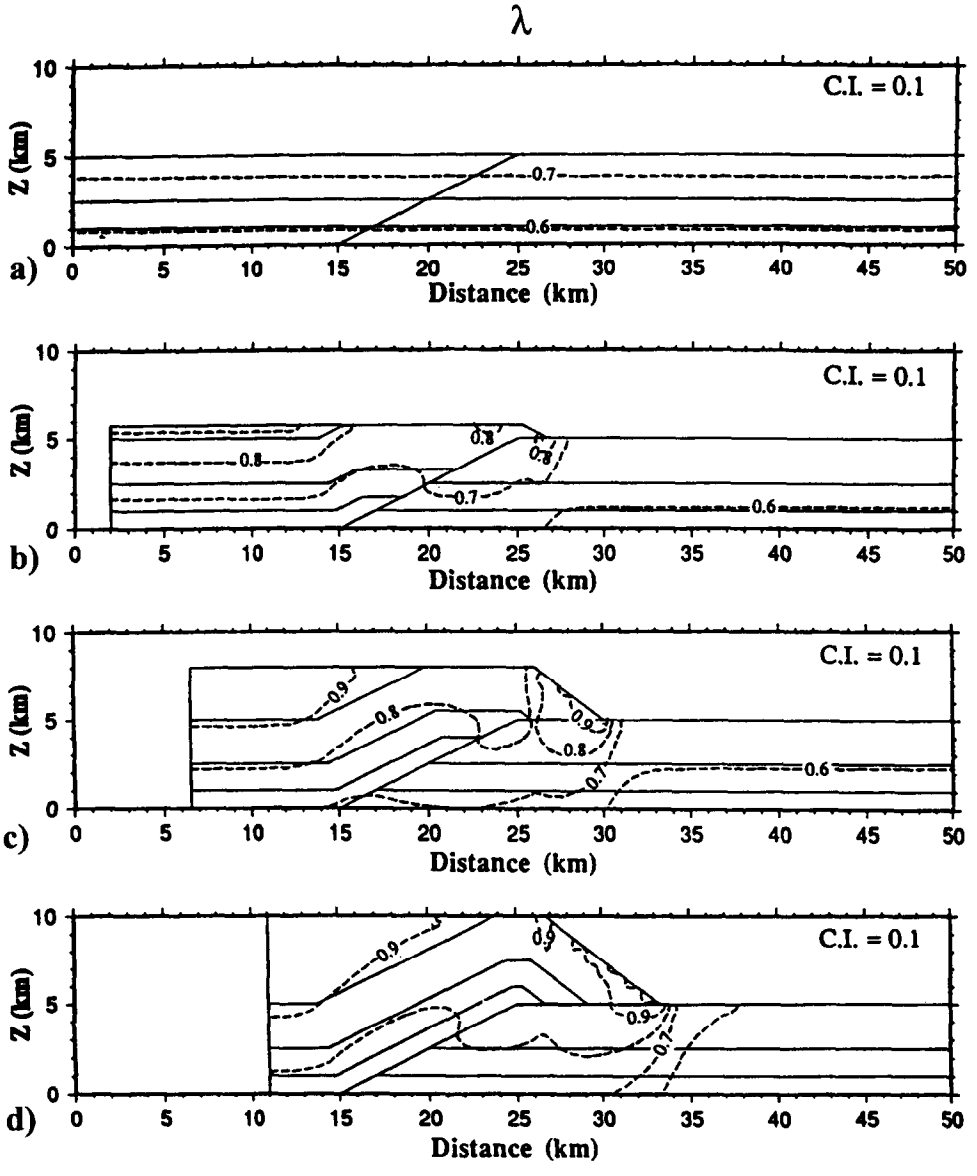

Fig. 7. Evolution of the ratio of pore pressure to lithostatic pressure within a thrust sheet with homogeneous and isotropic permeability of 10^{-18} m^2 and all other material parameters at standard values (Table 1). (a) Prior to thrusting, after deposition. (b) After 2 km of motion (18% of total). (c) After 6.5 km (60%). (d) At the end of thrusting where the section at the top of the ramp is doubled. The small contour loops at the top of the model are an artifact of both the node spacing and contouring rapidly changing small numbers, not numerical instability.

than fluid flow can dissipate them. Thus, siltstones, mudstones and shales which have permeabilities generally less than 10^{-16} m^2 (Fig. 1b) will be likely zones of over-pressuring during thrust loading; and sandstones and permeable carbonates which generally have permeabilities greater than 10^{-16} m^2 (Fig. 1b) will be likely zones where excess pore pressure gradients are relatively low due to dissipation by fluid flow.

Porosity compressibility (α_n) numerical experiments

Extremes of high porosity compressibility (1×10^{-8} Pa^{-1}) and low porosity compressibility (0 Pa^{-1}) were tested for a thrust belt with a homogeneous permeability of 10^{-18} m^2. The effect of doubling the porosity compressibility from the assumed standard of 5×10^{-9} Pa^{-1} to 1×10^{-8} Pa^{-1} had the effect of raising the excess pore pressure slightly throughout the model but most noticeably beneath the thrust sheet and hinterland syntectonic sediments (Fig. 11). Values of λ were also correspondingly higher (Fig. 12) for a higher compressibility, but the overall spatial distribution of λ contours was unchanged. For the incompressible rock porosity scenario ($\alpha_n = 0$ Pa^{-1}), the porosity parameter, b, was made zero so that porosity would not change as a function of effective stress. In this scenario, no excess pore pressure developed anywhere in the model. Therefore, the compression of pore space due to loading is the dominant factor in thrust belt pore pressure generation. Thermal expansion of the pore fluids is a lesser factor, incapable of generating any excess pore pressures when the permeability is 10^{-18} m^2 or more.

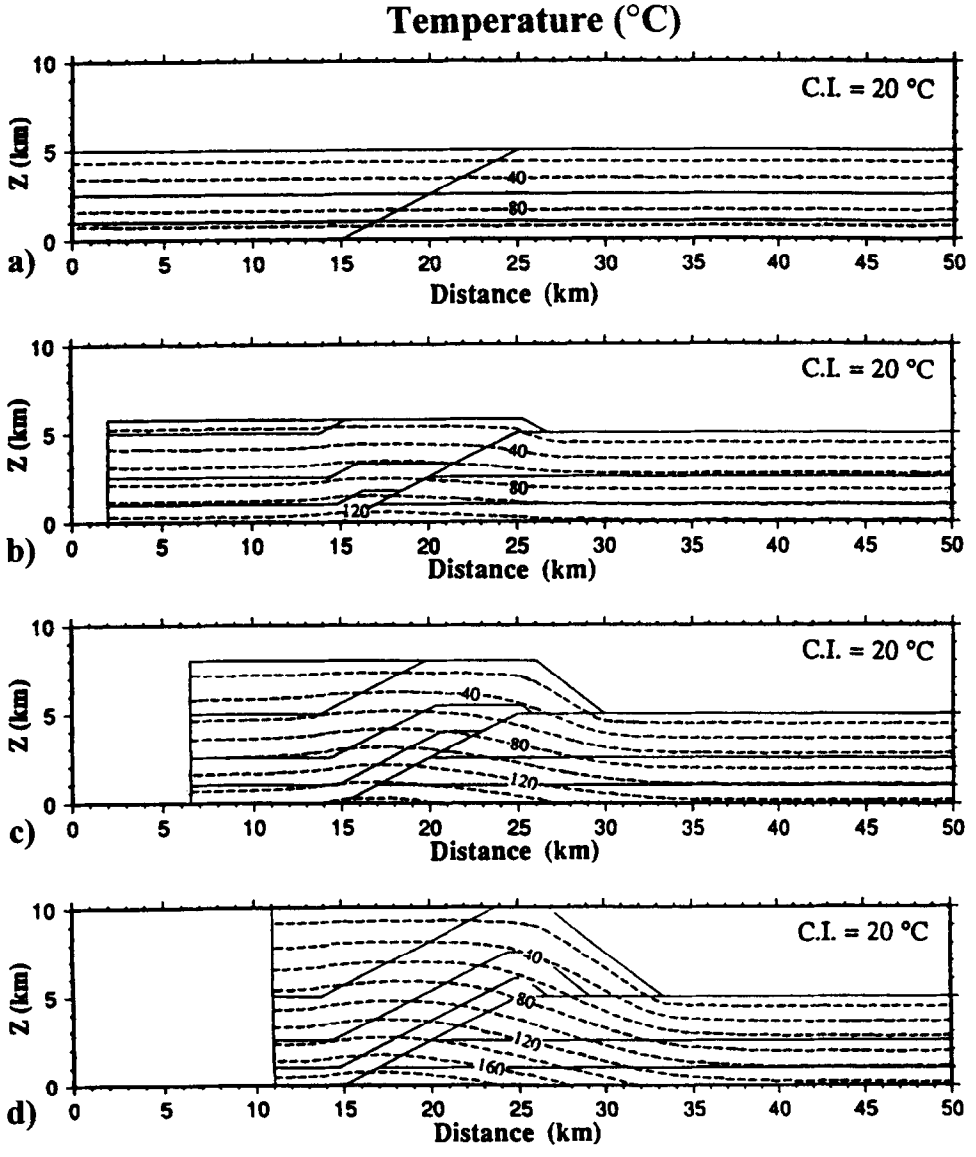

Fig. 8. Evolution of temperature within a thrust sheet with homogeneous and isotropic permeability of 10^{-18} m^2 and all other material parameters at standard values (Table 1). (a) Prior to thrusting, after deposition. (b) After 2 km of motion (18% of total). (c) After 6.5 km (60%). (d) At the end of thrusting where the section at the top of the ramp is doubled.

Inhomogeneous permeability numerical experiments

Four numerical experiments were run to test the effect of inhomogeneous permeability on the evolution of pore pressure using the generic North American stratigraphy developed earlier. As discussed previously, it was not possible to assign a single value of permeability to a lithologic layer based upon assumed lithologic characteristics alone. Therefore, two scenarios were tested in which (1) the permeability of Layers 1, 2 and 3 were 10^{-20}, 10^{-16}, and 10^{-18} m^2, respectively, and (2) the permeability of Layers 1, 2 and 3 were 10^{-18}, 10^{-14}, and 10^{-16} m^2, respectively.

Excess pore pressure for the two low permeability inhomogeneous thrust sheet scenarios were relatively high (Fig. 13b) in comparison to the homogeneous isotropic case (Fig. 13a). The low permeability Layer 1 tended to have the greatest excess pore pressure gradients and the high permeability Layer 2 had the lowest excess pore pressure gradients. In many places, the excess pore pressure contours were overturned near or within Layer 2 due to permeability contrasts. Layer 2 acted as a conduit for relatively rapid fluid flow because of its high permeability. Since fluid flow in Layer 2 was faster than flow in the isotropic Layer 3, fluid transported by Layer 2 tended to pond beneath Layer 3 generating zones of high pore pressure and high λ (Fig. 14b) within the fault bend anticline and beneath the thrust toe (Fig. 13b) in comparison to the homogeneous isotropic case (Fig. 14a). Thus, two distinct zones that are likely to produce fractures developed due to this permeability inhomogeneity. The evolution of λ is shown in Fig. 15.

The high permeability scenario produced very little excess pore pressure and most of this was in the lower model shale layer (Figs. 13c and 14c).

These results suggest it is necessary that a low permeability cap be present in the upper portion of the model so that high pore pressures can be trapped within

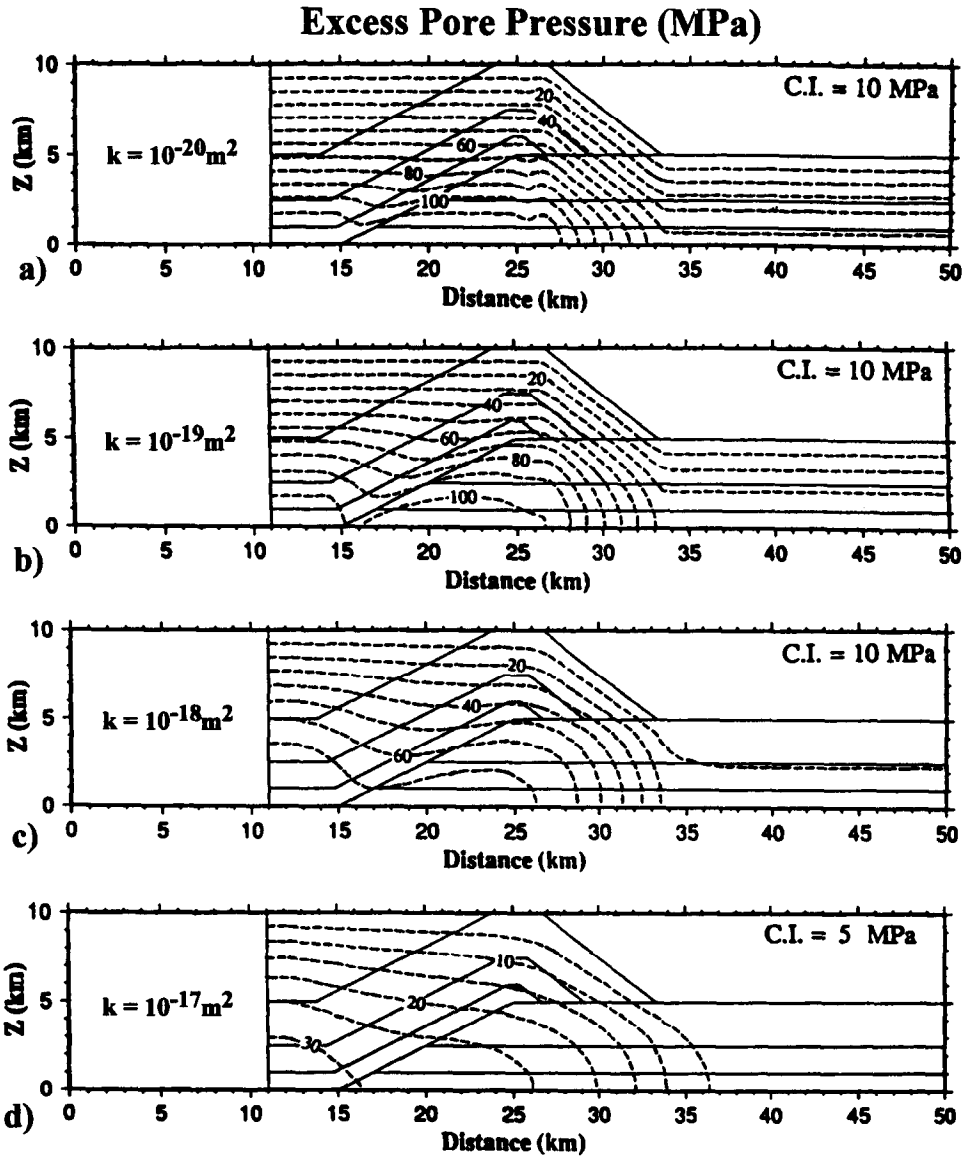

Fig. 9. Excess pore pressure for the final stage of thrust loading for four thrust sheets with different homogeneous and isotropic permeabilities ranging from 10^{-20} to 10^{-17} m^2.

the thrust sheet. A thin, low permeability unit near the base of the model overlain by relatively permeable units could not, by itself, generate pore pressures much over hydrostatic.

DISCUSSION

The results of models suggest that a critical factor in the generation of excess pore pressure in thrust belts is the presence of low permeability layers to restrict the rate of vertical fluid flow. The model in which the upper four fifths of the sedimentary column had permeabilities of the order of 10^{-16} m^2 or greater produced virtually no excess pore pressures because no low permeability layers were present to prevent the dissipation of high pore pressures to the surface boundary by vertical fluid flow. This high permeability scenario is considered to be highly unlikely because thrust sheets are composed of many layers of various lithologies (Smith 1992) whose permeabilities probably range over many orders of magnitude (Fig. 1b). Thus, Layer 2 which has been modeled as high permeability carbonates may contain layers of very low permeability, fine grained carbonates or even thin shale or siltstone layers which act as barriers to fluid flow. Therefore, the lower permeability thrust sheet scenario (Figs. 13b and 14b) is more likely than the higher permeability scenario which in turn suggests that high excess pore pressures are likely to develop in thrust sheets.

Clearly, the spatial distribution of permeability is a very important factor in determining the magnitude and distribution of excess pore pressures within thrust belts. In this study we have characterized permeability distribution for thrust sheets based upon lithologic characteristics. Real world thrust sheets undoubtedly have a much more complex permeability distribution than the model thrust sheet (compare the two parts of Fig. 1). As the scale of observation is increased to the dimensions of individual beds, many alternating high and low perme-

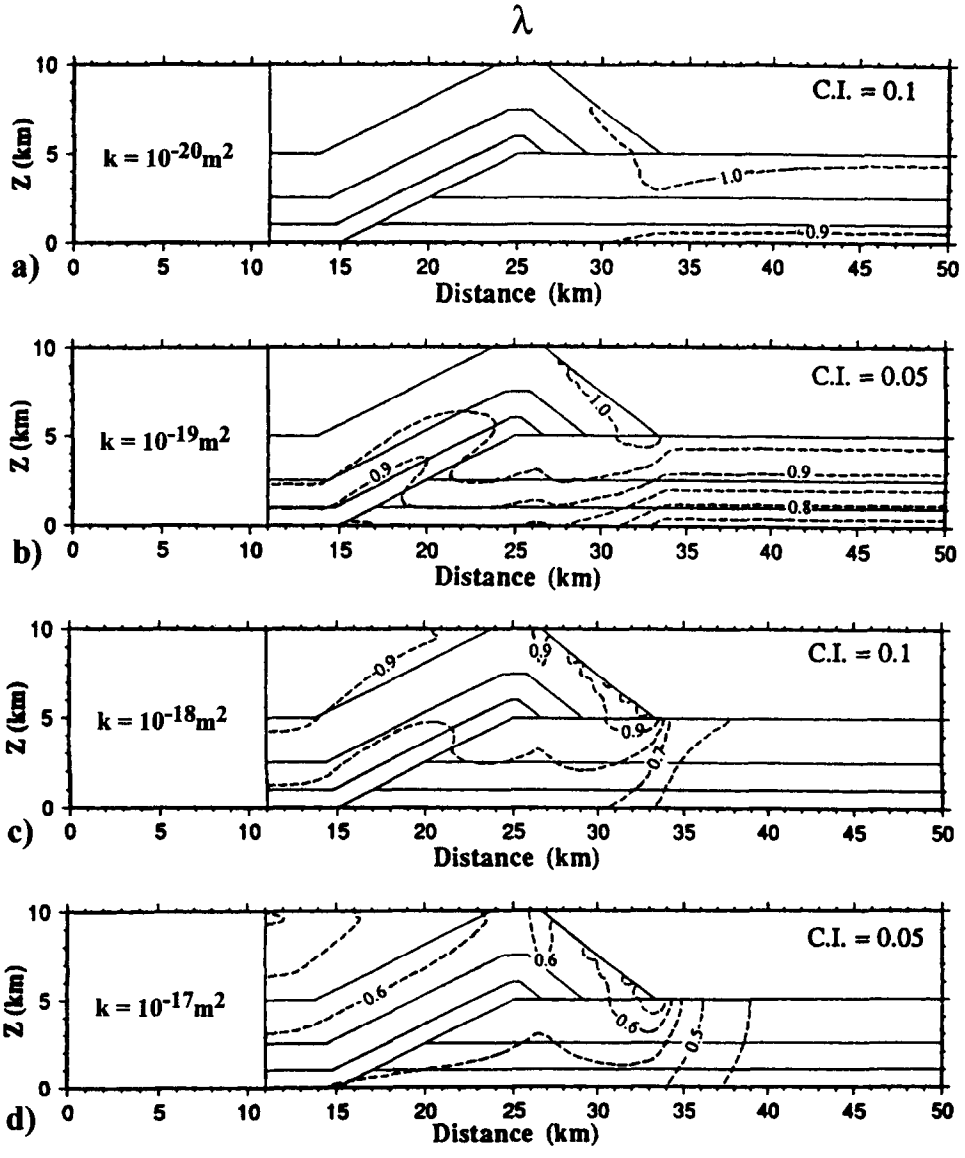

Fig. 10. Ratio of pore pressure to lithostatic pressure for the final stage of thrust loading for four thrust sheets with different homogeneous and isotropic permeabilities ranging from 10^{-20} to 10^{-17} m^2.

ability units will be observed. Therefore, the excess pore pressure distributions due to permeability inhomogeneities and/or anisotropies within real world thrust sheets are likely to be more complex than those within the model thrust sheets depending on the scale of observation.

Fault zone properties

The models of this study do not allow for separate hydrologic properties of the thrust fault. Instead, the fault is assumed to be a simple discontinuity separating the moving hanging wall from the stationary footwall. However, there is evidence that this assumption may not be valid. Faults have been noted to act as barriers to (Morrow *et al.* 1984, Morris & Wallace 1986) and conduits for fluid flow (Kerrich 1986, Morris & Wallace 1986). For accretionary prisms in particular, the latter evidence consists of observations of surface venting of fluids associated with thrust faults (Kulm *et al.* 1986, Carson *et al.* 1990, Henry *et al.* 1990, Kulm & Suess 1990), heat flow anomalies along thrust faults (Fisher & Hounslow 1990, Foucher *et al.* 1990), and geochemical evidence (Elderfield *et al.* 1990, Gieskes *et al.* 1990). Pumping and other tests in the Barbados accretionary prism suggested that the basal fault is highly permeable (Moore *et al.* 1982, 1990). Isotopic evidence (Bradbury & Woodwell 1987) from the rocks involved in thrusting of the front ranges of the Southern Canadian Rockies suggests that the major thrust sheets there behaved as separate hydrodynamic units perhaps because the thrust faults acted as barriers across which fluid could not readily flow.

Enhanced fluid flow along the thrust fault would tend to reduce pore pressures along the fault and within the surrounding rocks (Forster 1991, Ge & Garven 1994). If flow were restricted across the fault, pore pressure build up within the loaded sedimentary rocks beneath the thrust would tend to be trapped beneath the thrust fault. This could possibly increase the pore pressures beneath the thrust while reducing pressures above the thrust.

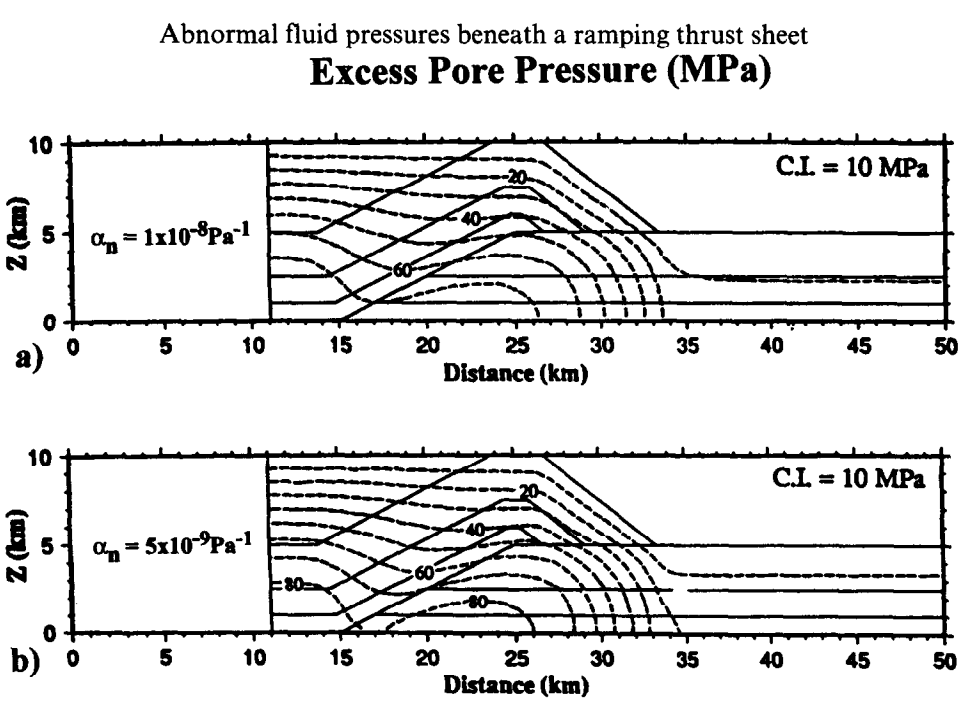

Fig. 11. Excess pore pressure for the final stage of thrust loading for three thrust sheets with different values of the porosity compressibility (α_n).

The low permeability basal unit in Figs. 13(b) and 14(b) reduces fluid flow across the thrust fault, and thus, approximates the presence of a low permeability fault zone. No concentrations of high excess pore pressure or high λ values are present beneath the low permeability layer along the thrust ramp.

Fracture and fault formation

Results concerning fracture and fault formation are not presented in this study due to the lack of coupling of the pore pressure equations with a complete description of the stress state of a ramping thrust sheet. However, it is possible that the effects of stress that have been neglected by this study could be very important in the evolution of excess pore pressures in thrust belts. As noted earlier, there must be some upper limit of pore pressures due to limitations in the strength of the rocks. Clearly, some failure criterion is needed to model fracture porosity and permeability changes which are likely to dissipate high pore pressures during rock failure. It is possible that pore pressure evolution along a thrust fault is cyclical, with pore pressures building due to increased horizontal compression until failure occurs which then reduces pore pressures by increasing fluid flow. As pore pressures are reduced, fractures close due to lack of pore pressure

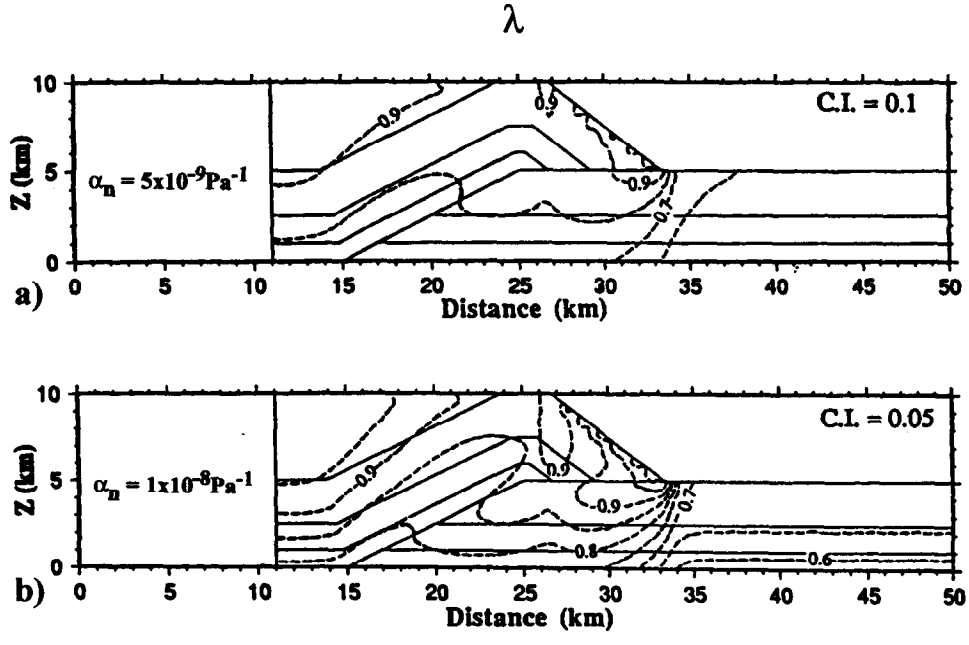

Fig. 12. Ratio of pore pressure to lithostatic pressure for the final stage of thrust loading for three thrust sheets with different values of the porosity compressibility (α_n).

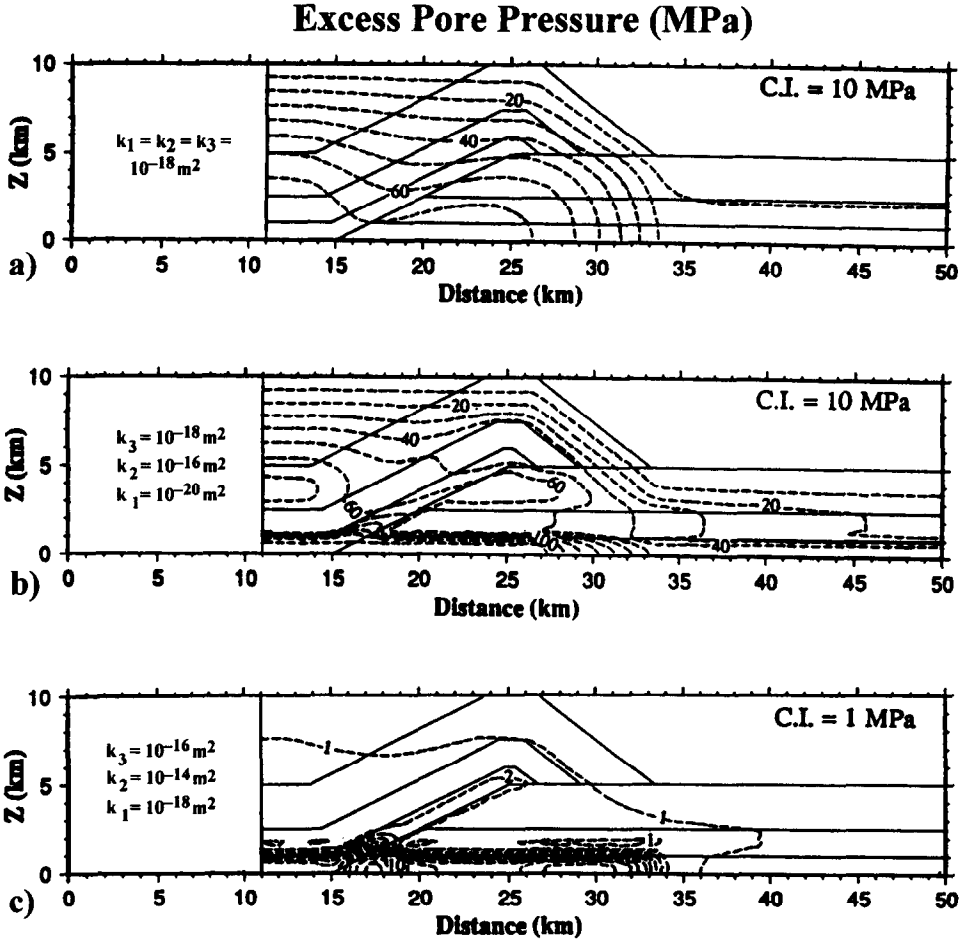

Fig. 13. Excess pore pressure for the final stage of thrust loading for three thrust sheets. (a) Standard homogeneous, isotropic thrust sheet. (b) Inhomogeneous, isotropic thrust sheet with permeabilities of 10^{-20}, 10^{-16} and 10^{-18} m^2 for Layers 1, 2 and 3, respectively. (c) Inhomogeneous, isotropic thrust sheet with permeabilities of 10^{-18}, 10^{-14} and 10^{-16} m^2 for Layers 1, 2 and 3, respectively.

to hold them open, and the cycle begins again. The impact of including fracture development on the models presented in this study could be great because at present the pore pressure is allowed to go beyond the mean stress with no upper limit imposed. Therefore, rather than a gradual increase in pore pressures with time, pore pressures may increase and decrease cyclically during thrust deformation. This mechanism could reduce the extremely high λ values that evolved in some of the models of this study.

It is possible to draw some conclusions about fracture formation from our models in the absence of a complete description of the stress state within the model thrust sheet by assuming that areas with high λ values ($\lambda > 1$) are likely zones for rock failure. Thus, for the inhomogeneous permeability model of the generic North American stratigraphy (Figs. 13 and 14), the hinge of the fault bend anticline and the interface of Layers 2 and 3 of the footwall beneath the thrust toe are the two likely zones where fracture could occur. Therefore, one might expect that real rocks in similar locations should contain a significant density of fractures and/or veins. If the models presented in Figs. 13(b) & (c) and 14(b) & (c) were run forward, the zone of high λ in the anticlinal hinge would probably decay somewhat due to lack of further syntectonic deposition (and therefore loading) behind the anticline due to cessation of vertical motion of the thrust sheet. The zone of high λ within and beneath the thrust toe would migrate with the toe and increase in magnitude or remain stable due to continuation of loading of the footwall beneath the moving thrust toe. Thus, further thrust motion would result in decreased fracturing in the rocks moving through the hinge of the anticline and forelandward migration of fracturing within the footwall rocks beneath the thrust toe.

In addition to fracture and vein development, zones of high λ could be locations where initiation of a new thrust fault begins. Therefore, a new thrust fault may initiate within the ramp anticline of the hanging wall, or beneath the thrust toe. The magnitudes of λ for the two high λ zones are of roughly equal magnitude for the isotropic, inhomogeneous thrust sheet during all stages of thrust loading (Fig. 15), and λ values approaching 1 do not develop until late in the model's evolution. That λ values are nearly equal for each high λ zone suggests that either zone is a likely location for a new thrust ramp to form. That λ is always greater near the surface at the thrust toe than in the anticlinal hinge suggests that a new thrust fault is likely to initiate first at the surface at the toe of the thrust sheet and propagate downward through the footwall. This conclusion was reached by other means by Goff & Wiltschko (1992) employing a mechanical

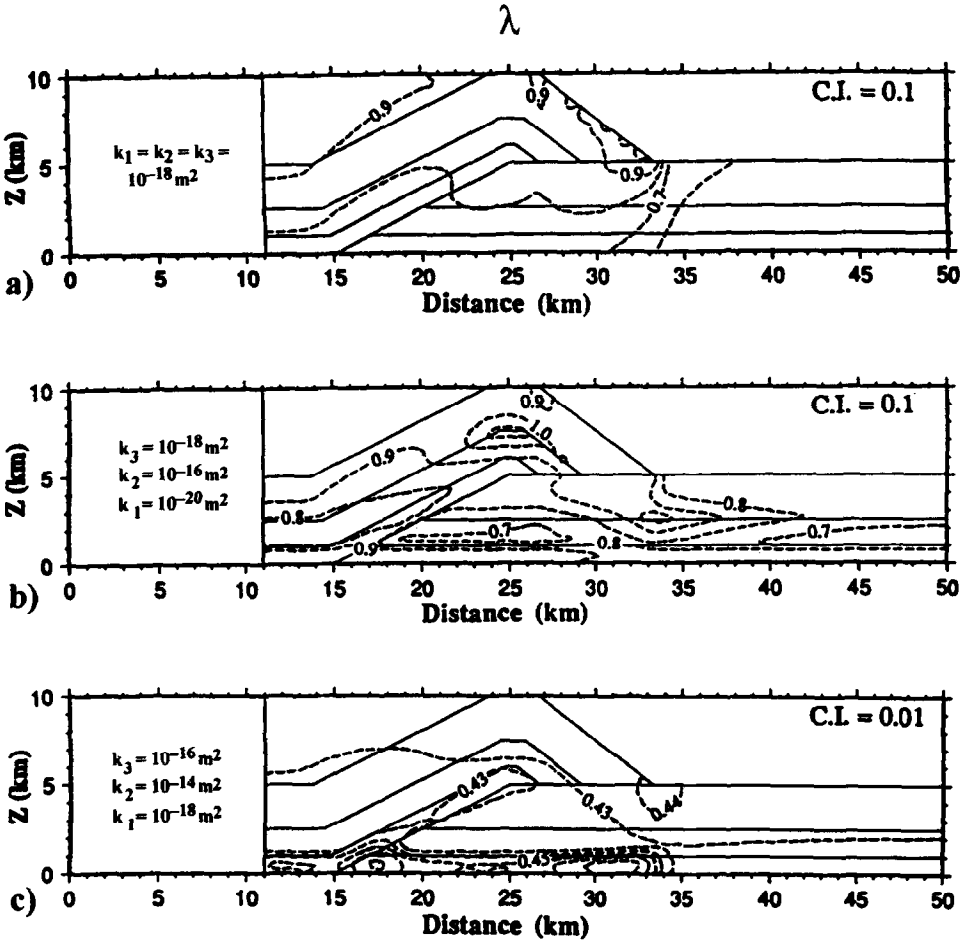

Fig. 14. Ratio of excess pore pressure to lithostatic pressure for the final stage of thrust loading for three thrust sheets. (a) Standard homogeneous, isotropic thrust sheet. (b) Inhomogeneous, isotropic thrust sheet with permeabilities of 10^{-20}, 10^{-16} and 10^{-18} m^2 for Layers 1, 2 and 3, respectively. (c) Inhomogeneous, isotropic thrust sheet with permeabilities of 10^{-18}, 10^{-14} and 10^{-16} m^2 for Layers 1, 2 and 3, respectively.

analysis which did not consider fluid pressure.

For the inhomogeneous case, a new thrust fault is likely to form somewhere within the footwall beneath the toe of the thrust sheet. However, it is a common observation that thrust ramps nucleate well in front of the previously moving thrust sheet. This observation may be in error due to post thrusting erosion removing the most frontal portion of the original upper plate. Nevertheless, if one accepts the observation at face value then a possible solution to this discrepancy may be found by considering the effects on the evolution of excess pore pressures of: (1) erosion of the ramping thrust sheet and, (2) subsequent deposition of eroded sediments on the footwall in front of the thrust sheet. The moving thrust sheet modeled in our study is assumed to experience no change in stress except by deposition in the hinterland region behind the fault bend fold anticline. In the absence of any loading, one would expect no excess pore pressures to evolve within the thrust sheet except by diffusion across the thrust fault from the footwall. With erosion, unloading of the thrust sheet would occur, and thus, loading of the footwall would be reduced. The effect of this unloading would likely be similar to a reduced rate of thrust sheet velocity; that is, pore pressures would be reduced throughout the model. The eroded material would be deposited in front of the eroding thrust sheet, loading the footwall beyond the edge of the thrust toe. The ability of the hinterland deposition loading in the models of this study to generate high pore pressures suggests that deposition in front of the thrust sheet could be significant in increasing the pore pressures beneath a syntectonic sedimentary apron in front of the thrust toe. Therefore, the deposition of a sedimentary apron in front of the thrust toe combined with erosion of the thrust toe could reduce λ values within and below the thrust toe while increasing λ values in front of the thrust toe in the footwall beneath the sedimentary apron. Erosion and redeposition in this manner could lead to more widely spaced thrust ramps.

CONCLUSIONS

In this study, numerical models were used to explore the evolution of excess pore pressures within thrust sheets. The major conclusions of this study are as follows.

(1) It is possible to generate pore pressures approaching lithostatic pressure within thrust sheets for reasonable assumptions about the conditions thought to have existed in thrust belts.

(2) Whether or not excess pore pressures can develop

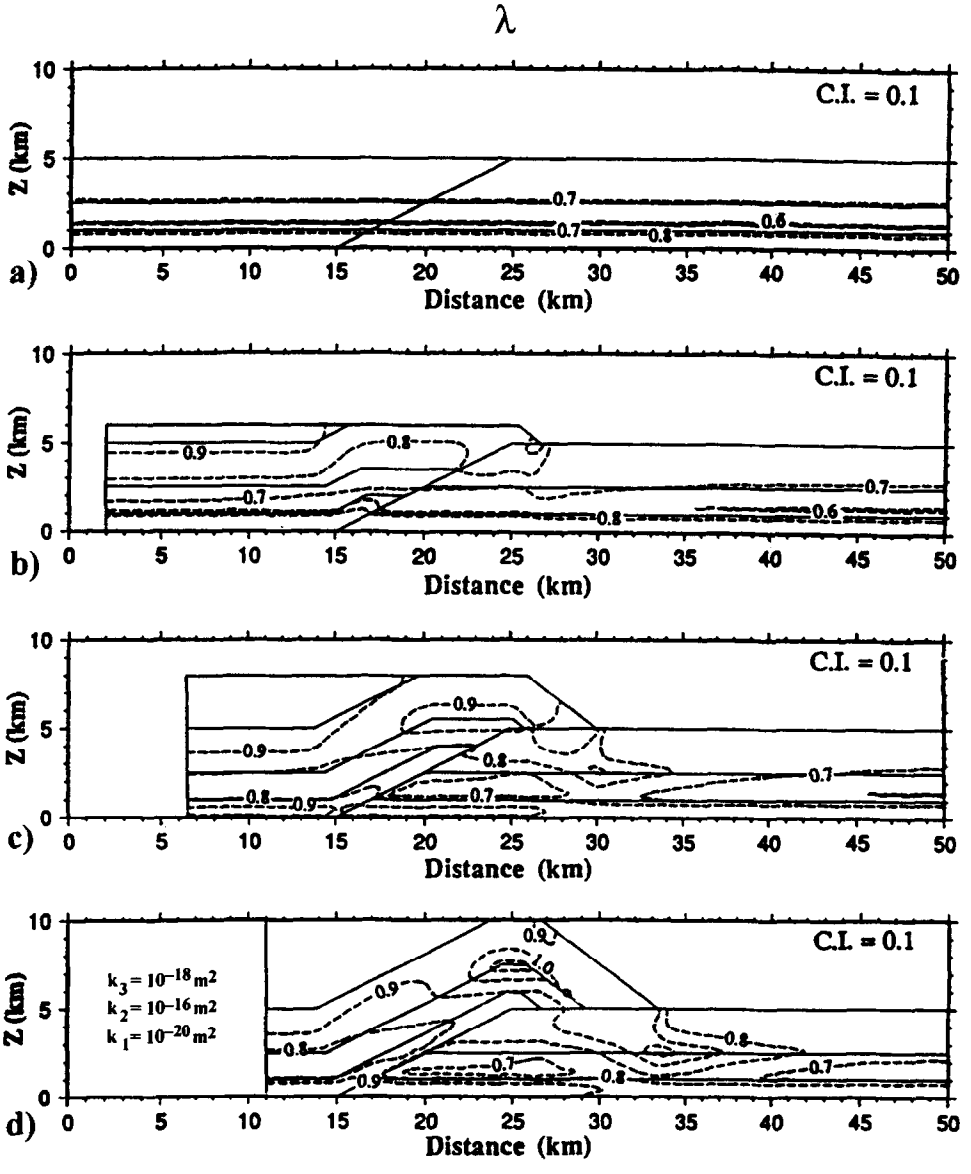

Fig. 15. Evolution of the ratio of pore pressure to lithostatic pressure for an isotropic, inhomogeneous thrust sheet with permeabilities of 10^{-20}, 10^{-16}, and 10^{-18} m^2 for Layers 1, 2 and 3, respectively. Sequence begins with the end of depositional loading.

in a thrust sheet is highly dependent upon the permeability of the rocks because permeability for common sedimentary rocks can vary over twelve orders of magnitude. In general, excess pore pressure generation by compression will exceed pore pressure dissipation by fluid flow for permeabilities less than approximately 10^{-16} m^2. Permeabilities greater than approximately 10^{-16} m^2 cause the rate of pore pressure dissipation to exceed pore pressure generation, thus producing hydrostatic pore pressure gradients.

(3) An important element required to generate excess pore pressure is the presence of low permeability layers to trap excess pore pressures in higher permeability layers below.

(4) Pore pressures approaching lithostatic can be generated within sedimentary rocks from depositional loading alone prior to thrusting, setting up in advance the conditions thought necessary for thrusting to begin.

(5) The highest pore pressures relative to overburden stress during thrusting will concentrate near the surface within and below the thrust toe and beneath areas of syntectonic sediment deposition.

(6) Excess pore pressure generation is dominated by compression of the pore space due to increasing mean stress. Thus, the porosity compressibility of rocks and the rate of mean stress increase are important physical parameters in determining the magnitude of excess pore pressure generation in thrust sheets.

(7) Generation of excess pore pressures by thermal expansion of the fluids is insignificant compared to pore pressure generation by compression of the pore space due to deposition or thrust loading. In the absence of porosity compression, thermal effects alone cannot generate excess pore pressures faster than fluid flow can dissipate them for at least permeabilities on the order of 10^{-18} m^2 or greater.

(8) Advective thermal flux by fluid flow does not alter the thermal gradient for the range of permeabilities used in this study.

(9) The inhomogeneous nature of the permeability for

thrust belts must be taken into account in correctly modelling pore pressure evolution within thrust sheets. The presence of a vertically inhomogeneous sequence of rocks thought to be representative of some North American thrust belts severely altered the pattern of excess pore pressure as compared to the homogeneous case. Most notably, a high permeability unit was found to act as a conduit for fluid flow which caused high λ values to concentrate at the top of the high permeability layer if a relatively low permeability layer was present above it. The highest λ values were concentrated within the fault bend anticline and beneath the thrust sheet toe.

(10) The base of the upper plate may strengthen with time relative to elsewhere in the upper plate because fluid pressure is reduced there by fluid flow into the lower plate.

Acknowledgements—This material is based upon work supported under a National Science Foundation Fellowship, a scholarship from the Society of Exploration Geophysicists, and a student research grant from the Geological Society of America to RES. We appreciate a grant of computer time on the Cray supercomputer from the Texas A & M Supercomputer Center. DVW acknowledges the support of NSF grants EAR89-16784 and EAR92-19986 and many discussions with Pat Domenico. Our understanding of the material derivative was advanced by discussions with Brann Johnson. We would like to thank Don Fisher for a thought provoking review which led to significant improvement in the manuscript.

REFERENCES

Axen, G. J. 1984. Thrusts in the eastern Spring Mountains, Nevada: Geometry and mechanical implications. *Bull. geol. Soc. Am.* **95**, 1202–1207.

Bear, J. 1972. *Dynamics of Fluids in Porous Media.* Elsevier, New York.

Birch, F. 1966. Compressibility; elastic constants. In: *Handbook of Physical Constants* (edited by Clark, S. P.). *Geol. Soc. Am. Memoir* **97**, 107–173.

Bott, M. H. P. 1971. *The Interior of the Earth.* St. Martin's Press, New York.

Brace, W. F. 1980. Permeability of crystalline and argillaceous rocks: a review. *Int. J. Rock Mech. Min. Sci.* **17**, 241–251.

Bradbury, H. J. & Woodwell, G. R. 1987. Ancient fluid flow within foreland terrains. In: *Fluid flow in Sedimentary Basins and Aquifers* (edited by Goff, J. C. & Williams, B. P. J.). *Spec. Publs geol. Soc. Lond.* **34**, 87–102.

Brock, W. G. & Engelder, T. 1977. Deformation associated with the movement of the Muddy Mountain overthrust in the Buffington window, southeastern Nevada. *Bull. geol. Soc. Am.* **88**, 1667–1677.

Carson, B., Suess, E. & Strasser, J. C. 1990. Fluid flow and mass flux determinations at vent sites on the Cascadia Margin accretionary prism. *J. geophys. Res.* **95**, 8891–8898.

Chan, Y. C. 1964. Preliminary study on the geothermal gradients and formation or reservoir pressures of gas and oil fields in northern Taiwan. *Petrol. Geol. Taiwan* **3**, 127–139.

Clark, S. P. 1966. Thermal conductivity. In: *Handbook of Physical Constants* (edited by Clark, S. P.). *Geol. Soc. Am. Memoir* **97**, 459–482.

Clauser, C. 1992. Permeability of crystalline rocks. *EOS, Trans., Am. Geophys. Union* **73**, 233–237.

Dahlen, F. A. 1984. Noncohesive critical Coulomb wedges: an exact solution. *J. geophys. Res.* **89**, 10,125–10,133.

Dahlen, F. A., Suppe, J. & Davis, D. 1984. Mechanics of fold-and-thrust belts and accretionary wedges: cohesive coulomb theory. *J. geophys. Res.* **89**, 10,087–10,101.

Davis, D., Suppe, J. & Dahlen, F. A. 1983. Mechanics of fold-and-thrust belts and accretionary wedges. *J. geophys. Res.* **88**, 1153–1172.

Davis, S. N. 1969. Porosity and permeability of natural materials. In: *Flow Through Porous Media* (edited by DeWiest, R. J. M.). Academic Press, New York, 54–89.

Daw, G. P., Howell, F. T. & Woodward, F. A. 1974. The effect of applied stress upon the permeability of some Permian and Triassic sandstones of northern England. *Advances in Rock Mechanics, Proceedings of the Third International Congress of Rock Mechanics,* vol. (IIA), 537–542.

DiTullio, L. & Byrne, T. 1990. Deformation paths in the shallow levels of an accretionary prism: the Eocene Shimanto belt of southwest Japan. *Bull. geol. Soc. Am.* **102**, 1420–1438.

Domenico, P. A. & Schwartz, F. W. 1990. *Physical and Chemical Hydrogeology.* John Wiley & Sons, New York.

Elderfield, H., Kastner, M. & Martin, J. B. 1990. Compositions and sources of fluids in sediments of the Peru subduction zone. *J. geophys. Res.* **95**, 8819–8828.

Elliott, D. 1976. The motion of thrust sheets. *J. geophys. Res.* **81**, 949–963.

Englund, K. J. 1964. *Geologic Map of the Middlesboro South Quadrangle, Tennessee–Kentucky–Virginia.* U.S. Geol. Surv. Map GQ-301, scale 1:24,000.

Englund, K. J., Roen, J. B. & DeLaney, A. O. 1964. *Geologic Map of the Middlesboro North Quadrangle, Kentucky.* U.S. Geol. Surv. Map GQ-300, scale 1:24,000.

Fisher, A. T. & Hounslow, M. W. 1990. Transient fluid flow through the toe of the Barbados accretionary complex: constraints from Ocean Drilling Program leg 110 heat flow studies and simple models. *J. geophys. Res.* **95**, 8845–8858.

Forster, C. B. 1991. Impact of a permeable thrust fault on thermal and hydrologic regimes: regional-scale numerical modelling results. *Geol. Soc. Am., Abstracts with Programs* **23**, 104.

Foucher, J. P. 1990. Heat flow, tectonics and fluid circulation at the toe of the Barbados Ridge accretionary prism. *J. geophys. Res.* **95**, 8859–8868.

Ge, S. & Garven, G. 1992. Hydromechanical modeling of tectonically driven groundwater flow with application to the Arkoma foreland basin. *J. geophys. Res.* **97**, 9119–9144.

Ge, S. & Garven, G. 1994. A theoretical model for thrust-induced deep groundwater expulsion with application to the Canadian Rocky Mountains. *J. geophys. Res.* **99**, 13,851–13,868.

Gieskes, J. M., Vrolijk, P. & Blanc, G. 1990. Hydrogeochemistry of the Northern Barbados accretionary complex transect: Oceanic Drilling Project leg 110. *J. geophys. Res.* **95**, 8809–8818.

Goff, D. F. & Wiltschko, D. V. 1992. Stresses beneath a ramping thrust sheet. *J. Struct. Geol.* **14**, 437–450.

Gregory, A. R. 1977. Aspects of rock physics from laboratory and log data that are important to seismic interpretation. *Mem. Am. Ass. Petrol. Geol.* **26**, 15–46.

Gretener, P. E. 1972. Thoughts on overthrust faulting in a layered sequence. *Bull. Can. Petrol. Geol.* **20**, 583–607.

Gretener, P. E. 1977. On the character of thrust faults with particular reference to basal tongues. *Bull. Can. Petrol. Geol.* **25**, 110–122.

Gretener, P. E. 1981. Pore pressure, discontinuities, isostasy and overthrust: In: *Thrust and Nappe Tectonics* (edited by McClay, K. R. & Price, N. J.). *Spec. Publs geol. Soc. Lond.* **9**, 33–39.

Harris, L. D. & Milici, R. L. 1977. Characteristics of thin-skinned style of deformation in the Southern Appalachians, and potential hydrocarbon traps. *U.S. Geol. Survey Prof. Paper* **1018**, 40.

Hedberg, H. D. 1936. Gravitational compaction of clays and shales. *Am. J. Sci.* **31**, 241–287.

Henry, P. 1990. Mud volcano field seaward of the Barbados accretionary complex: a deep-towed side scan sonar survey. *J. geophys. Res.* **95**, 8899–8916.

Henry, P. & Wang, C. Y. 1991. Modeling of fluid flow and pore pressure at the toe of Oregon and Barbados accretionary wedges. *J. geophys. Res.* **96**, 20109–20130.

Hoholick, J. D., Metarko, T. & Potter, P. E. 1984. Regional variation of porosity and cement: St. Peter and Mount Simon sandstones in Illinois Basin. *Bull. Am. Ass. Petrol. Geol.* **68**, 753–764.

Hsü, K. J. 1969. Role of cohesive strength in the mechanics of overthrust faulting and landsliding. *Bull. geol. Soc. Am.* **80**, 927–952.

Hubbert, M. K. & Rubey, W. W. 1959. Role of fluid pressure in mechanics of overthrust faulting: Part I, Mechanics of fluid filled porous solids and its application to overthrust faulting. *Bull. geol. Soc. Am.* **70**, 115–166.

Jones, F. O., Jr. 1975. A laboratory study of the effects of confining pressure on fracture flow and storage capacity in carbonate rocks. *J. Petrol. Tech.* **27**, 21–27.

Jordan, T. E., Allmendinger, R. W., Damanti, J. F. & Drake, R. E. 1993. Chronology of motion in a complete thrust belt; the

Precordillera, 30–31°S. Andes Mountains. *J. Geol.* **101**, 135–156.
Kerrich, R. 1986. Fluid infiltration into fault zones: chemical, isotopic, and mechanical effects. *Pure & Appl. Geophys.* **124**, 225–268.
Kuan, M. Y. 1967. Comparative study of the gas reservoirs in the Chinshui and Tiehchenshan gas fields, Miaoli, Taiwan. *Petrol. Geol. Taiwan* **5**, 151–190.
Kuan, M. Y. 1968. Lower Miocene gas reservoirs of the oil and gas fields in the Miaoli area, Taiwan. *Petrol. Geol. Taiwan* **6**, 157–182.
Kuan, M. Y. 1971. Advanced study of the subsurface geology of the Chinshui gas field, Miaoli, Taiwan. *Petrol. Geol. Taiwan* **8**, 47–64.
Kulm, L. D. 1986. Oregon subduction zone: venting, fauna and carbonates. *Science* **231**, 561–566.
Kulm, L. D. & Suess, E. 1990. Relationship between carbonate deposits and fluid venting: Oregon accretionary prism. *J. geophys. Res.* **95**, 8899–8916.
Lewis, C. R. & Rose, S. C. 1970. A theory relating high temperatures and overpressures. *J. Petrol. Tech.* **22**, 11–16.
Lide, D. R. 1991. *CRC Handbook of Chemistry and Physics*, 72nd edn. CRC Press, Boston.
Merewether, E. A., Blackmon, P. D. & Webb, J. C. 1984. The mid-Cretaceous Frontier Formation near Moxa Arch, Southern Wyoming. *U.S. Geol. Survey Prof. Pap.* **1290**, 29.
Moore, J. C. 1982. Offscraping and underthrusting of sediment at the deformation front of the Barbados Ridge: Deep Sea Drilling Project leg 78A. *Bull. geol. Soc. Am.* **93**, 1065–1077.
Moore, J. C., Orange, D. & Kulm, L. D. 1990. Interrelationship of fluid venting and structural evolution: Alvin observations from the frontal accretionary prism, Oregon. *J. geophys. Res.* **95**, 8795–8808.
Moore, J. C. & Vrolijk, P. 1992. Fluids in accretionary prisms. *Rev. Geophys.* **30**, 113–136.
Mordecai, M. & Morris, L. H. 1971. An investigation into the changes of permeability occurring in a sandstone when failed under triaxial stress condition. In: *Dynamic Rock Mechanics* (edited by Clark, G. B.). *Proc. 12th Symposium of Rock Mechanics*, American Institute of Mining, Metallurgical and Petroleum Engineers, 221–240.
Morris, H. T. & Wallace, R. E. 1986. Characteristics of faults and shear zones in deep mines. *Pure & Appl. Geophys.* **124**, 107–126.
Morrow, C. A., Shi, L. Q. & Byerlee, J. D. 1984. Permeability of fault gouge under confining pressure and shear stress. *J. geophys. Res.* **89**, 3193–3200.
Palciauskas, V. V. & Domenico, P. A. 1989. Fluid pressures in deforming porous rocks. *Water Resourc. Res.* **25**, 203–213.
Paterson, M. S. 1978. *Experimental Rock Deformation—The Brittle Field.* Springer-Verlag, New York.
Perrodon, A., Masse, P. 1984. Subsidence, sedimentation and petroleum systems. *J. Petrol. Geol.* 7, 5–26.
Rich, J. L. 1934. Mechanics of low-angle overthrust faulting as illustrated by Cumberland thrust block, Virginia, Kentucky, and Tennessee. *Bull. Am. Ass. Petrol. Geol.* **18**, 1584–1596.
Rubey, W. W. & Hubbert, M. K. 1959. Role of fluid pressure in mechanics of overthrust faulting: Part II, Overthrust belts in geosynclinoria of western Wyoming in light of fluid–pressure hypothesis. *Bull. geol. Soc. Am.* **70**, 167–206.
Schmoker, J. W. & Halley, P. B. 1982. Carbonate porosity versus depth: a predictable relation for south Florida. *Bull. Am. Ass. Petrol. Geol.* **66**, 2561–2570.
Shi, Y. & Wang, C. Y. 1986. Pore pressure generation in sedimentary basins: overloading versus aquathermal. *J. geophys. Res.* **91**, 2153–2162.
Shi, Y. & Wang, C. Y. 1987. Two-dimensional modeling of the P–T–t paths of regional metamorphism in simple overthrust terrains. *Geology* **15**, 1048–1051.
Shi, Y. & Wang, C. Y. 1988. Generation of high pore pressures in accretionary prisms: inferences from the Barbados subduction complex. *J. geophys. Res.* **93**, 8893–8910.
Smith, G. D. 1985. *Numerical Solution of Partial Differential Equations: Finite Difference Methods.* Oxford University Press, New York.
Smith, R. E. 1992. One- and two-dimensional finite difference models of pore pressure evolution within and below a moving thrust sheet. Unpublished MSc Thesis, Texas A & M University, College Station, Texas, 165 pp.
Strauss, J. M. & Schubert, G. 1977. Thermal convection of water in a porous medium: effects of temperature and pressure dependent thermodynamic and transport properties. *J. geophys. Res.* **82**, 325–333.
Suppe, J. & Wittke, J. H. 1977. Abnormal pore-fluid pressures in relation to stratigraphy and structure in the active fold-and-thrust belt of northwestern Taiwan. *Petrol. Geol. Taiwan* **14**, 11–24.
Suppe, J. 1983. Geometry and kinematics of fault-bend folding. *Am. J. Sci.* **283**, 684–721.
Thayer, P. A. 1983. Relationship of porosity and permeability to petrology of the Madison Limestone in rock cores from three test wells in Montana and Wyoming. *U.S. Geol. Surv. Prof. Paper* **1273-C**.
Touloukian, Y. S., Judd, W. R. & Roy, R. F. 1981. *Physical Properties of Rocks and Minerals*, vol. II-2, McGraw-Hill, New York.
Turcotte, D. L. & Schubert, G. 1982. *Geodynamics: Applications of Continuum Physics to Geological Problems.* John Wiley & Sons, New York, 450 pp.
Wang, C. Y. & Shi, Y. 1986. Evolution of pore pressures in the fold-and-thrust belt of western Taiwan. *Acta Geol. Taiwanica* **24**, 211–236.
Wang, C. Y. 1990. Hydrogeologic processes in the Oregon–Washington accretionary complex. *J. geophys. Res.* **95**, 9009–9024.
Westbrook, G. K. & Smith, M. J. 1983. Long decollements and mud volcanoes: evidence from the Barbados Ridge Complex for the role of high pore–fluid pressure in development of an accretionary complex. *Geology* **11**, 279–283.
Wilhelm, B. & Somerton, W. H. 1967. Simultaneous measurement of pore and elastic properties of rocks under triaxial stress condition. *J. Soc. Petrol. Eng.* **7**, 283–294.
Wiltschko, D. V. & Dorr, J. A. 1983. Timing of deformation in overthrust belt and foreland of Idaho, Wyoming, and Utah. *Bull. Am. Ass. Petrol. Geol.* **67**, 1304–1322.
Winslow, M. A. 1983. Clastic dike swarms and structural evolution of foreland fold and thrust belt of the southern Andes. *Bull. geol. Soc. Am.* **94**, 1073–1080.
Zoback, M. D. & Byerlee, J. D. 1976. Effect of high-pressure deformation on permeability of Ottawa sand. *Bull. Am. Ass. Petrol. Geol.* **60**, 1531–1542.